



AMERICAN UNIVERSITY OF BEIRUT

KINETIC AND ADSORPTIVE CHARACTERIZATION OF  
BIOCHARS IN ZINC, COPPER AND LEAD METAL IONS  
REMOVAL USING BATCH AND CONTINUOUS SYSTEMS

by  
MAHA MILED ABDALLAH

A thesis  
submitted in partial fulfillment of the requirements  
for the degree of Master of Science  
to the Department of Chemical and Petroleum Engineering  
of the Maroun Semaan Faculty of Engineering and Architecture  
at the American University of Beirut

Beirut, Lebanon  
May 2018

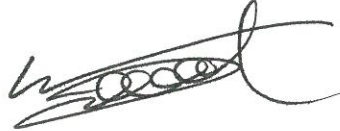
AMERICAN UNIVERSITY OF BEIRUT

KINETIC AND ADSORPTIVE CHARACTERIZATION OF  
BIOCHARS IN ZINC, COPPER AND LEAD METAL IONS  
REMOVAL USING BATCH AND CONTINUOUS SYSTEMS

by  
MAHA MILED ABDALLAH

Approved by:

Walid Saoud



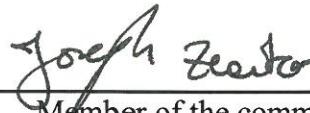
08 May 2018

On behalf of:

Dr. Mohammad N Ahmad, Professor, Chairman  
Department of Chemical engineering

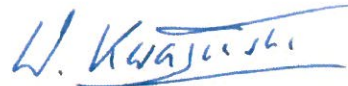
Advisor

Dr. Joseph Zeaiter, Associate Professor  
Department of Chemical engineering



Member of the committee

Dr. Witold Kwapinski, Senior Lecturer  
Department of Chemical Sciences, University of Limerick, Ireland



Member of the committee

Date of thesis defense: April 18, 2018

# AMERICAN UNIVERSITY OF BEIRUT

## THESIS, DISSERTATION, PROJECT RELEASE FORM

Student Name:

Abdallah \_\_\_\_\_ Maha \_\_\_\_\_  
Last First Middle

Master's Thesis       Master's Project       Doctoral Dissertation

I authorize the American University of Beirut to: (a) reproduce hard or electronic copies of my thesis, dissertation, or project; (b) include such copies in the archives and digital repositories of the University; and (c) make freely available such copies to third parties for research or educational purposes.

I authorize the American University of Beirut, to: (a) reproduce hard or electronic copies of it; (b) include such copies in the archives and digital repositories of the University; and (c) make freely available such copies to third parties for research or educational purposes after:

**One ---- years from the date of submission of my thesis, dissertation, or project.**

**Two ---- years from the date of submission of my thesis, dissertation, or project.**

**Three ---- years from the date of submission of my thesis, dissertation, or project.**



Signature

9 May 2018

Date

## ACKNOWLEDGMENTS

I would like to express my deepest gratitude for Prof. Mohammad Ahmad for the amazing opportunity in the Erasmus+ International Mobility Credit to complete my thesis work.

I would also like to thank Prof. Witold Kwapinski and James J. Leahy for their recommendations, support and help in completing this work at the University of Limerick.

Special thanks to Prof. Joseph Zaeiter for being a member of my thesis committee.

I would also like to show deep gratitude and appreciation to my family members, my mother, father and sister, and my friends for their daily support.

# AN ABSTRACT OF THE THESIS OF

Maha Miled Abdallah for Master of Sciences  
Major: Chemical Engineering

Title: Kinetic and adsorptive characterization of Biochars in Zinc, Copper and Lead metal ions removal using batch and continuous systems

Spent mushroom compost biochar (SMCB) and coconut shell biochar (CB) were prepared by carbonisation and tested for the removal of heavy metals: Zn(II), Cu(II) and Pb(II) by adsorption. They were characterized to determine their physical and chemical properties. The adsorption of heavy metals was evaluated by studying several factors, such as the initial solution pH, contact time, temperature and competitive adsorption. The effect of initial solution pH was initially studied and it was found that at a pH of 6 the highest metal removal took place for the adsorption using both biochars. Kinetic and equilibrium studies were carried out to determine the mechanism involved during adsorption. Pseudo-second order and Langmuir model most accurately described the adsorption process, showing that chemisorption takes place on a monolayer, homogenous and energetically-equivalent adsorption sites. The Weber-Morris model demonstrated the significance of intra-particle diffusion on the adsorption process. In addition, thermodynamic studies showed that the process is endothermic, favorable, with good affinity of metals to the biochar.

SMCB and CB were used as adsorbent in a continuous fixed-bed column. The breakthrough curve was obtained for each heavy metal and the Thomas and Clark models were fitted to further understand the breakthrough behavior. When all three metals co-exist, competitive adsorption took place in both batch and continuous systems, showing that Pb has higher affinity to SMCB than Cu and Zn.

## NOMENCLATURE

$b$	Langmuir constant
$B$	Clark model characteristic parameter
$BTC$	Breakthrough Curve
$CEC$	Cation Exchange Capacity
$C_0$	Initial concentration (mg/L)
$C_a$	Concentration of the adsorbate on the adsorbent (mg/L)
$C_e$	Concentration at equilibrium of the sorbate in the solution (mg/L)
$C_{in}$	Inlet concentration (mg/L)
$CI/CM$	Clark model
$C_{out}$	Outlet concentration (mg/L)
$C_t$	Concentration at time t (mg/L)
$h$	Amount of sorbate per adsorbent mass and time (mg/L.g.min)
$k_1$	First-order rate constant ( $\text{min}^{-1}$ )
$k_2$	Second-order rate constant ( $\text{g.mg}^{-1}.\text{min}^{-1}$ )
$K_e$	Thermodynamic equilibrium constant
$K_f$	Fruendlich constant
$k_i$	Intra-particle Weber-Morris rate constant ( $\text{mg.g}^{-1}.\text{min}^{-1/2}$ )

$K_L$	Constant characteristic of the Langmuir isotherm (L/mg)
$k_T$	Thomas rate constant (L/min.mg)
$m$	Mass of biochar used (g)
$n$	Freundlich constant
$PFO$	Pseudo-first order
$pH_e$	pH at equilibrium
$pH_{in}$	Initial pH
$pH_{pzc}$	pH value at the point of zero charge
$PSO$	Pseudo-second order
$q_0$	Maximum adsorption capacity, characteristic of the Langmuir isotherm (mg/g)
$q_e$	Adsorption capacity at equilibrium (mg/g)
$q_{max}$	Maximum adsorption concentration in the solid phase, obtained using the Thomas model (mg/L)
$q_t$	Adsorption capacity at time t (mg/g)
$r$	Clark model characteristic parameter ( $\text{min}^{-1}$ )
$R$	Gas constant (=8.314 J/mol.K)
$R_L$	Separation factor
$SMCB$	Spent Mushroom Compost Biochar
$T$	temperature ( $^{\circ}\text{C}$ )
$t$	Time (min)



$Th/TM$	Thomas model
$V$	Sample volume (L)
$WM$	Weber-Morris model

### **Greek Symbols**

$\beta$	Thickness at the boundary layer during adsorption (m)
$\Delta G^\circ$	Change in Gibbs free energy (kJ/mol)
$\Delta H^\circ$	Change in enthalpy (kJ/mol)
$\Delta pH$	Change in pH
$\Delta S^\circ$	Change in entropy (kJ/mol)
$v$	Volumetric flowrate (L/min)

### **Subscripts**

$1$	Pseudo-first order
$2$	Pseudo-second order
$e$	equilibrium
$i$	Intra-particle diffusion
$max$	Maximum
$pzc$	Point of zero charge

# CONTENTS

ACKNOWLEDGMENTS.....	v
ABSTRACT.....	vi
NOMENCLATURE.....	vii
LIST OF ILLUSTRATIONS.....	xii
LIST OF TABLES.....	xiv
Chapter	
I. BIOCHARS FOR THE ADSORPTION OF HEAVY METALS.....	1
A. Heavy metals in the environment.....	1
B. Biochars for heavy metal removal.....	3
C. Spent mushroom compost and coconut shell derived biochars.....	5
D. Fixed bed column adsorption.....	6
II. EXPERIMENTAL METHODOLOGY AND MATHEMATICAL MODELS.....	8
A. Material preparation.....	8
B. Characterization of SMCB.....	8
C. Kinetics test.....	10
D. Thermodynamics test.....	12
E. Adsorption isotherms.....	13
F. Fixed-bed column design.....	15

G. Fixed-bed column adsorption modeling.....	16
<b>III. RESULTS AND DISCUSSION.....</b>	<b>17</b>
A. Characterization of SMCB and CB.....	17
B. Cation Exchange Capacity.....	24
C. Effect of initial pH.....	25
D. Adsorption isotherms.....	30
E. Adsorption kinetics.....	34
F. Effect of temperature.....	42
G. Column adsorption modeling.....	45
H. Competitive adsorption: batch and continuous systems.....	48
<b>IV. CONCLUSION.....</b>	<b>55</b>
<b>BIBLIOGRAPHY.....</b>	<b>56</b>

## ILLUSTRATIONS

Figure	Page
1. FTIR spectra of SMCB before adsorption, and after adsorption of Zn, Cu and Pb.....	22
2. FTIR spectra of CB before adsorption, and after adsorption of Zn, Cu and Pb.....	23
3. pH changes during metal ions adsorption on SMCB.....	28
4. pH changes during metal ions adsorption on CB.....	28
5. Percent of ions removal using SMCB as a function of initial pH.....	29
6. Percent of ions removal using CB as a function of initial pH.....	29
7. Adsorption isotherms of (a) Zn, (b) Cu and (c) Pb on SMCB.....	32
8. Adsorption isotherms of (a) Zn, (b) Cu and (c) Pb on CB.....	33
9. Kinetics for heavy metals ions (a) Zn, (b) Cu and (c) Pb adsorption on SMCB at various temperatures, experimental data described by pseudo-first order (PFO) and pseudo-second order (PSO).....	37
10. Kinetics for heavy metals ions (a) Zn, (b) Cu and (c) Pb adsorption on CB for the experimental data described by pseudo-first order (PFO) and pseudo-second order (PSO).....	38
11. Kinetics for heavy metals ions (a) Zn and (b) Cu adsorption on SMCB at various temperatures, experimental data described by intra-particle diffusion Weber-Morris (WM) model.....	41
12. Kinetics for heavy metals ions Zn and Cu adsorption on CB with the experimental data described by intra-particle diffusion Weber-Morris (WM) model.....	42
13. Experimental continuous adsorption $C_t/C_0$ as a function of time in a single metal system for (a) Zn, (b) Cu and (c) Pb, described by the Thomas (Th) and Clark (Cl) models using SMCB.....	46
14. Experimental continuous adsorption $C_t/C_0$ as a function of time in a single metal system for (a) Zn, (b) Cu and (c) Pb, described by the Thomas (Th)	

and Clark (Cl) models using CB.....	47
15. Experimental $C_t/C_0$ as a function of time for Pb, Cu and Zn when mutually present in a tertiary system in a fixed-bed continuous adsorption using SMCB.....	54
16. Experimental $C_t/C_0$ as a function of time for Pb, Cu and Zn when mutually present in a tertiary system in a fixed-bed continuous adsorption using CB	54

## TABLES

Table		Page
1.	Heavy metal concentration range ( $\mu\text{g/L}$ ) for a wastewater before and after treatment in a Biological Wastewater Treatment Plant in Brazil.....	3
2.	Heavy metal concentration range ( $\text{mg/L}$ ) and their allowable safe limit for a wastewater before and after treatment Titagarh, India.....	3
3.	Selected properties of spent mushroom compost and coconut shell (raw material) and elemental analyses of SMCB and CB .....	20
4.	Langmuir and Freundlich isotherm parameters for the adsorption of heavy metals ions onto SMCB .....	31
5.	Langmuir and Freundlich isotherm parameters for the adsorption of heavy metals ions onto CB.....	31
6.	Kinetics parameters for the adsorption of heavy metals using SMCB at different temperatures.....	36
7.	Kinetics parameters for the adsorption of heavy metals using CB.....	37
8.	The Gibbs free energy change for each metal ions at different temperatures, enthalpy and entropy changes for each metal using SMCB.....	44
9.	The Gibbs free energy change for each metal ions at different temperatures, enthalpy and entropy changes for each metal using CB.....	44
10.	Thomas and Clark model parameters for fixed-bed column using SMCB.....	48
11.	Thomas and Clark model parameters for fixed-bed column using CB.....	48
12.	Adsorption capacities of the heavy metals ions in a tertiary component system using SMCB.....	51
13.	Adsorption capacities of the heavy metals ions in a tertiary component system using CB.....	52

## CHAPTER I

# BIOCHARS FOR THE ADSORPTION OF HEAVY METALS

### A. Heavy metals in the environment

Highly hazardous contaminants, such as heavy metals, are generated by a number of industrial processes and released into the environment in wastewater. Heavy metals present in the wastewater can be absorbed by plants and thus affect humans and living organisms [1]. They include lead, cadmium, zinc, copper, mercury, nickel, arsenic and several others. Their concentration beyond specific limits becomes highly toxic as they can be incorporated into vegetation and aquatic organisms and eventually into the food chain. Thus, heavy metals not only lead to pollution of water and soil, but also pose severe risks to all living organisms [2].

Lead is a naturally occurring metal in the environment. However, many agricultural and industrial applications including ammunitions, batteries, metal production and mining, cause its release in high concentrations into the environment [3]. Chronic and acute exposure to lead affects the brain, kidney, blood and the metabolism of vitamin D [4]. Its maximum permissible contamination level is 10  $\mu\text{m/L}$  according to World Health Organization (WHO), which has been exceeded in water supplied for household use, in for example: coastal Madagascar; groundwater in Lagos; and waters downstream of mines in Avoca, Glendalough and Silvermines in Ireland. [5-7].

Even though copper and zinc are essential elements for human beings, their excess concentration in plants and food can lead to toxicity [8]. They are generated by milling, electroplating, metal treatment, mining and several other industrial activities [9]. The concentration of these two metals was significantly high in surface waters downstream of mines in Tynagh and Glandore, Ireland [7]. Table 1 shows the concentration of different heavy metals present in a wastewater before and after treatment in a Biological Wastewater Treatment Plant in Brazil [10]. We can see that after treatment of this wastewater, the concentration of heavy metals decreased but did not drop to traces, mainly for manganese, lead and zinc. However, their upper limit after treatment was shown to be within the safe limit permitted by EPA and US legislations [10]. Another example is shown in Table 2 for the heavy metal concentration in treated and untreated wastewater in Titagarh, India [11]. The upper range of heavy metal concentrations is shown to be higher than the allowable safe limit for almost all heavy metal for both treated and untreated wastewater. This shows that even with the current implemented techniques used to treat wastewater, the heavy metals are not efficiently removed from wastewater. Therefore, it is highly important to develop a suitable low-cost technique that reduces the pollution of soil and water by heavy metals.



Table 1: Heavy metal concentration range ( $\mu\text{g/L}$ ) for a wastewater before and after treatment in a Biological Wastewater Treatment Plant in Brazil [10]

	Concentration ( $\mu\text{g/L}$ )						
	Cd	Cr	Cu	Mn	Hg	Pb	Zn
Untreated	0.06-	2.11-	10.66-	47.83-	0.00-	9.66-	36.80-
water	1.19	20.73	28.50	61.79	0.50	334.00	236.50
Treated	0.04-	1.68-	2.13-	35.55-	0.00-	4.22-	22.80-
water	0.11	13.53	19.87	73.41	0.24	76.42	76.25

Table 2: Heavy metal concentration range (mg/L) and their allowable safe limit for a wastewater before and after treatment Titagarh, India [11]

	Concentration (mg/L)					
	Cd	Cr	Cu	Ni	Pb	Zn
Untreated	0.00-	0.00-	0.07-	0.00-	0.00-	0.21-
water	0.06	0.81	6.30	4.20	7.50	4.30
Treated	0.00-	0.00-	0.01-	0.04-	0.00-	0.10-
water	0.03	0.36	5.81	6.80	0.24	3.90
Safe Limit	0.01	0.10	0.20	0.20	0.50	2.00

## B. Biochars for heavy metal removal

The use of biochars, non-toxic by-products generated from agriculture waste [12] can replace some more expensive adsorbents used for the decontamination of

water. Biochar is a product formed during the carbonisation of biomass by pyrolysis. Its properties are similar to those of charcoal as it contains high amount of organic carbon and including aromatic structures that enhance the adsorption capacity of the biochar. Any kind of biomass can be used in the production of biochars, each having different properties [13]. Biochars have a lower surface area and porosity compared to activated carbon, however, they have a higher content of oxygen-containing acid groups that increase the metal sorption efficiency [14, 15]. The use of biochars as low-cost adsorbents has been widely investigated in order to replace activated carbons in the decontamination of wastewater. These carbon-rich porous solid can be obtained from biomass and bio-organic wastes [16]. The thermal decomposition of biomass derived from plants leads to high aromatic carbon groups in the biochar, due to the presence of high amount of lignin and cellulose. It provides the biochar with a higher stability and an increased resistance to microbial decomposition [17, 18]. Hence, the use of biochars has shown to be an effective solution for the management of biological wastes and the treatment of wastewater. Thus, the biochar pore and surface structure depend on the carbonisation conditions and the biomass structure and composition.

Previous studies were done to investigate the maximum adsorption capacity of different lignocellulosic biochars for heavy metal removal. The maximum adsorption capacity for Pb removal was shown to be 22.85 mg/g, 39.37 mg/g and 76.6 mg/g using different biochars derived from apricot stone [19], soybean hulls [20] and pecan shell [21], respectively. Agoubordea and Navia used sawdust and brine sediments derived biochars [22] for the removal of Zinc (2.58 and 4.85 mg/g, respectively) and Copper (2.31 and 4.69 mg/g, respectively). Nasernejad et al. investigated the use of biochars

derived from carrot residues and treated with HCl. The maximum adsorption capacity was shown to be 45.09, 29.61 and 32.74 mg/g for Cr, Zn and Cu removal, respectively [23]. In addition, Park et al. investigated the use of sesame straw biochars and the maximum adsorption capacity was 102, 86, 65, 55 and 34 mg/g for the removal of Pb, Cd, Cr, Cu and Zn, respectively [24]. Therefore, biochars have been shown to be effective adsorbents in the application of wastewater treatment for the removal of heavy metal cations.

### **C. Spent mushroom compost and coconut shell derived biochars**

Spent mushroom compost is the residual compost waste obtained after the mushroom crop has been harvested. 1 kg of mushrooms can result in approximately 5 kg of spent mushroom compost [25]. More than  $3.5 \cdot 10^6$  tons of spent mushroom compost are generated annually in the European Union and an estimate of 295,000 tons is produced yearly by the Irish mushroom industry [26, 27]. Spent mushroom compost contains a significant amount of organic nutrients as it is produced from wheaten straw, poultry manure, gypsum mixed with cottonseed and mushroom waste. Therefore, their composition, high abundance and low-cost have attracted much attention for their application as biomass [28].

The yearly production of coconut is approximated to be 5.5 million tons. 1.94 million hectares of coconut are cultivated in India, leading to approximately 15,840 million nuts [29]. Thus, a significant loss in coconut is resulted from their shedding of buttons and thus a considerable amount is discarded as waste in agriculture [30]. Hence, it is highly important to manage this cheap waste in applications such as their

conversion into biochar material. This application would help minimize their disposal and make use of them in applications that help reduce water contamination.

Adsorption on sorbents prepared from agricultural or industrial by-products are reported to be promising materials for removing metal ions from aqueous solution [31]. In this study, the use of spent mushroom compost biochar (SMCB) and coconut shell biochar (CB) has been investigated for the adsorption of heavy metals: zinc Zn(II), copper Cu(II) and lead Pb(II). The effect of initial solution pH, adsorption kinetic at various temperature and the sorption isotherms of  $Zn^{2+}$ ,  $Cu^{2+}$  and  $Pb^{2+}$  were investigated, to establish the adsorption mechanism onto SMCB and CB.

#### **D. Fixed bed column adsorption**

As most studies are limited to batch adsorption, it is highly important to study the continuous adsorption to obtain accurate scale-up data for large scale of water treatment. Fixed-bed continuous adsorption was used to study the dynamic behavior in the column, which can be represented by the breakthrough curve (BTC) [32]. Fixed-bed adsorbents are highly adequate for the use of granular adsorbents in the removal of contaminants. In order to design an appropriate adsorption unit, preliminary studies must be performed to determine the optimal operating parameters and conditions [33, 34]. Fixed-bed adsorption depends on contact time and distance travelled by the influent solution. The sorbate ions will accumulate on the sorbent particles and equilibrium is reached layer by layer from the top to the bottom of the column [35]. Depending on the adsorption kinetics, a mass transfer zone is formed between the loaded sorbent particles and the unloaded ones. As the mass transfer zone moves downward in the column, the

concentration of sorbates in the effluent solution starts to increase, forming the breakthrough curve [36, 37]. The prediction of the breakthrough behavior is essential in the fixed-bed adsorber design. Several mechanistic models were developed to investigate the breakthrough and the mass transport mechanisms involved during adsorption [33]. In this study, two models were applied: the Thomas and Clark models. On the other hand, water treatment includes the removal of several metals simultaneously, which emphasizes the importance of competitive adsorption study. The co-existence of the three metals was investigated using the batch and continuous techniques.

In previous studies, different biochars were applied in a fixed bed column to remove heavy metal pollutants. Ding et al. reported that biochars derived from modified hickory chips removed 19.1, 17.9, 1.83, 0.98 and 0.89 mg/g of Pb, Cu, Zn, Cd and Ni, respectively [38]. In another study, *Tectona grandis* leaves biochars were used to remove Co and Ni with an adsorption capacity of 23.63 and 26.99 mg/g, respectively [39]. Park et al. used chicken bone biochars to remove Cu, Cd and Zn in a fixed-bed column and the adsorption capacities were 210, 192 and 178 mg/g, respectively [40]. In addition, dead calcareous skeleton biochars were used to remove Cd and Pb with a maximum adsorption capacity of 29.95 and 47.74 mg/g, respectively [41]. These results prove that in fact biochars are effective sorbents that could be used for heavy metal decontamination in both batch and continuous column adsorption techniques.

## CHAPTER II

# EXPERIMENTAL METHODOLOGY AND MATHEMATICAL MODELS

### A. Material preparation

Locally available spent mushroom compost and coconut shells were used in this study. The material was carbonised at a temperature of 500°C for 3 hours under oxygen-limited conditions using a Lenton furnace (laboratory chamber furnace). The SMCB was then ground and sieved to obtain fine granules of particle size between 0.180 and 0.425µm.

Stock solutions of CuCl<sub>2</sub> (>98% Merck part no. 8.18247.0500), ZnCl<sub>2</sub> (98% Aldrich Part no. 20.808-6) and Pb(NO<sub>3</sub>)<sub>2</sub> (99.5% Riedel de Haen part no. 11520) were prepared as sources of the metal ions Cu(II), Zn(II), and Pb(II) at a concentration of 3·10<sup>-3</sup> mol/L. 50 mL samples were prepared at a specific pH using sodium hydroxide Na(OH) and nitric acid HNO<sub>3</sub> (AnalaR NORMAPUR). Biochar (0.5g) was then added and the samples were shaken at a constant speed of 240 rpm using a magnetic stirrer.

### B. Characterization of SMCB

The total amount of C, H and N was analyzed using an elemental analyzer (Elemental Vario el Cube Analyzer). The moisture content of spent mushroom compost was obtained according to the standard: Solid recovered fuels — Determination of moisture content using the oven dry method ICS 75.160.10, DD CEN/TS 15414-1:2010.

The ash content for spent mushroom compost and SMCB was determined according to ICS 75.160.10, EN 14775:2009. The volatile matter was determined according to ICS 75.160.10, EN 15402:2011. The higher heating value was obtained using a Parr 6200 Calorimeter. The Brunauer-Emmet-Teller (BET) surface area of the biochar was determined using multi-point method (Autosorb-1 – Quantachrome Instruments, USA). Before analysis, samples were vacuum degassed at 200°C for 4-16 h. Degassing time varied based on the time necessary to reach a stable surface area measurement.

The surface functionality of the biochars surface before and after adsorption was investigated using a Fourier transform infrared (FTIR) spectroscopy (Cary 630 FTIR with MicroLab Software). The biochar samples were finely ground and analyzed at 8 cm<sup>-1</sup> resolution for a total of 32 sample scans, in the wave number range of 4000-650 cm<sup>-1</sup>.

SMCB and CB were also digested before and after adsorption to obtain the amount of metals present in the biochar. The solution was analyzed using Inductively Coupled Plasma spectrometry (Agilent ICP 5100 ICP-OES). Digestion was conducting by adding concentrated HNO<sub>3</sub> (3mL) and H<sub>2</sub>O<sub>2</sub> (12mL) to the biochar and heating at 120°C for 24 hours [42]. Subsequently, concentrated HF (4mL) was added followed by HNO<sub>3</sub> (2mL) and left at 70°C for 24 hours, to ensure that all solid biochar was in solution. Finally, 10mL of concentrated boric acid was added for neutralization. The solution was filtered and diluted to 50mL for analysis of elements using ICP.

The cation exchange capacity (CEC) of SMCB was determined by the replacement of the NH<sub>4</sub><sup>+</sup> ions with Na<sup>+</sup> ions. One gram of SMCB was added to a sodium acetate solution (20mL, 1.0M) to saturate the exchange sites. The solution was then

transferred to an extraction column containing cotton wool where it was leached using the same sodium acetate solution, then four times with ethanol (30 mL, 98%) until the conductivity of the extract was less than  $40 \mu\text{Scm}^{-1}$  to remove excess sodium acetate. The conductivity was measured using a Jenway 4510 conductivity meter. In order to replace the adsorbed  $\text{Na}^+$  ions, leaching with ammonium acetate (30 mL, 1.0M) was repeated three times. The extract was then analyzed using a Varian Spectra AA220 atomic absorption spectrophotometer (AAS) at a wavelength of 330.3 nm to determine the  $\text{Na}^+$  content and calculate the CEC [43].

### C. Kinetics test

50 mL samples of metal solutions ( $3 \cdot 10^{-3}$  mol/L) were prepared at a pH of 6 and shaken with 0.5g of SMCB using an IKA WERKE RT 15 power. Triplicate samples were taken with a syringe and filtered through a  $0.450 \mu\text{m}$  membrane filter and the concentration of the remaining metal ions was analyzed using AAS at a wavelength of 327.4 nm for Cu, 283.3 nm for Pb and 213.9 nm for Zn.

The adsorption capacity  $q_t$  (mg/g) was obtained according to the following eq. (1):

$$q_t = \frac{(C_0 - C_t)V}{m} \quad (1)$$

where  $C_0$  is the initial concentration of metal ion (mg/L),  $C_t$  is the concentration remaining of the metal ion (mg/L),  $V$  is the volume of the sample (L),  $m$  is the mass of the biochar in the sample (g).



Generally, adsorption equilibrium is not reached instantaneously for porous adsorbents. Thus, kinetic models were developed to study the rate of the mass transfer of ions from the aqueous solution into the adsorbent particles to reach the equilibrium state. In most cases, the adsorption rate is not limited by the external diffusion of ions to the surface of the adsorbent, but is instead controlled by solute transport into the interior of the adsorbent particle (intra-particle diffusion) [30]. Studies of the kinetic parameters of adsorption are important to determine the rate-limiting mass transfer mechanism and hence obtain the required contact time for fixed-bed reactors design.

The kinetic models investigated in this study are: pseudo-first order (PFO), pseudo-second order (PSO) and Weber-Morris (WM) model. The PFO model describes the rate of the liquid-solid phase adsorption system based on eq. (2) [44]:

$$\log(q_e - q_t) = \log(q_e) - \frac{k_1 t}{2.303} \quad (2)$$

where  $q_e$  and  $q_t$  represent the adsorption capacity (mg/g) at equilibrium and time  $t$  (min), respectively,  $k_1$  is the first-order rate constant ( $\text{min}^{-1}$ ).

Another kinetic model is based on the PSO rate law, described by eq. (3):

$$\frac{t}{q_t} = \frac{t}{q_e} + \frac{1}{h} \quad (3)$$

where  $k_2$  is the PSO rate constant ( $\text{g}\cdot\text{mg}^{-1}\cdot\text{min}^{-1}$ ) [44]. The amount of sorbate per adsorbent mass and time,  $h$ , can be obtained using eq. (4). It can be used to compare the sorption rate of the cations on SMCB at different process temperatures.

$$h = k_2 q_e^2 \quad (4)$$

The WB model was developed to investigate if the internal resistance is the limiting step, based on eq. (5) [45]:

$$q_t = k_i t^{1/2} + \beta \quad (5)$$

where  $k_i$  is the intra-particle WB rate constant ( $\text{mg}\cdot\text{g}^{-1}\cdot\text{min}^{-1/2}$ ) and  $\beta$  describes the thickness at the boundary layer during adsorption.

#### D. Thermodynamics test

The effect of temperature on the adsorption process was investigated by varying the adsorption temperature: 20°C, 40°C and 60°C. Thermodynamic parameters were obtained using the following eqs. (6-8) [46, 47]:

$$\Delta G^\circ = \Delta H^\circ - T\Delta S^\circ \quad (6)$$

$$\Delta G^\circ = -RT \ln(K_e) \quad (7)$$

$$\ln(K_e) = \frac{\Delta S^\circ}{R} - \frac{\Delta H^\circ}{RT} \quad (8)$$

where  $\Delta G^\circ$  is the Gibbs free energy change,  $\Delta H^\circ$  is the enthalpy change (kJ/mol),  $\Delta S^\circ$  is the entropy change (kJ/mol). R is the gas constant ( $8.314 \text{ J mol}^{-1}\text{K}^{-1}$ ) and T is the temperature of the adsorption process (K).  $K_e$  is the thermodynamic equilibrium constant, also defined as the distribution coefficient and can be determined using eq. (9):

$$K_e = \frac{C_a}{C_e} \quad (9)$$

where  $C_a$  is the equilibrium concentration of the adsorbate on the adsorbent (mg/L), and  $C_e$  is the equilibrium concentration of the adsorbate in solution (mg/L) [48].

These parameters are highly important to further understand the adsorption process. If the Gibbs free energy is negative, the adsorption is spontaneous and does not require external energy for the process to take place. In addition, a negative  $\Delta H^\circ$  value indicates that the adsorption is exothermic, while a positive value indicates endothermic adsorption. When adsorption takes place, an adsorbent-adsorbate complex is formed. A negative  $\Delta S^\circ$  implies that no significant modification occurs in the internal structure during the adsorption process and that an associative mechanism is involved. A positive  $\Delta S^\circ$  implies that during adsorption, a dissociative mechanism takes place and that the process is not favorable at high temperatures [49].

### **E. Adsorption isotherms**

The adsorption capacity of metal cations on the biochars can be analyzed using equilibrium isotherms. The most common models used for metal sorption are the Langmuir and Freundlich models. The Langmuir model is based on monolayer adsorption onto the homogeneous and energetically equivalent surface containing the adsorption sites, where once they are filled, no additional sorption can take place on this site. Therefore, the surface achieves a maximum adsorption when the saturation point is reached. This isotherm is represented by eq. (10)

$$q_e = \frac{q_0 K_L C_e}{1 + K_L C_e} \quad (10)$$

where  $C_e$  is the equilibrium concentration (mg/L),  $q_e$  is the amount adsorbed at equilibrium (mg/g),  $K_L$  (L/mg) and  $q_0$  (mg/g) are constants characteristics of the Langmuir equation. They can be obtained by plotting the specific adsorption ( $C_e/q_e$ ) as a function of  $C_e$ .

The Freundlich model is an empirical model that represents a multilayer adsorption onto a heterogeneous surface with varying affinities. The binding sites with a stronger affinity are occupied first and the energy of the sorption sites decreases with increasing site occupation until the adsorption process is completed. The eq. (11) represents this sorption isotherm:

$$q_e = K_f C_e^{1/n} \quad (11)$$

where  $n$  is a Freundlich constant and  $K_f$  is a temperature dependent constant. They can be obtained by plotting  $\ln(q_e)$  as a function of  $\ln(C_e)$  [50].

The separation factor  $R_L$  is determined to study the shape of the isotherm: unfavorable when  $R_L > 1$ , linear when  $R_L = 1$ , favorable when  $0 < R_L < 1$  and irreversible when  $R_L = 0$  [50].

$$R_L = \frac{1}{1 + bC_0} \quad (12)$$

where  $b$  is the Langmuir constant and  $C_0$  is the initial concentration of the adsorbate (mg/L).

To confirm the adsorption isotherms, equation (10) was used to calculate the surface area of the biochar after adsorption ( $S_A$ ) took place, in order to check if a monolayer is formed or not [51].

$$S_A = \frac{q_0 A_{MB} N_L}{MW} \quad (10)$$

where  $N_L$  is Avogadro's number ( $6.023 \times 10^{23}$  molecule/mole),  $MW$  is the molecular weight of the sorbed metal and  $A_{MB}$  is the surface area occupied by one molecule of the metal ion.  $A_{MB}$  is found to be 0.74, 0.71 and 0.84 Å for Zn, Cu and Pb ions respectively [52-53].

#### **F. Fixed-bed column design**

A laboratory-scale column is used to perform the adsorption of the heavy metals in a continuous system. Metal solutions were prepared at a concentration of  $3 \cdot 10^{-3}$  mol/L using  $Zn(Cl)_2$ ,  $Cu(Cl)_2$  and  $Pb(NO_3)_2$ . The same concentration is prepared when a mixture of the three metals is used. The column has a height of 25 cm and an inner diameter of 1.9 cm. Layers of glass beads were packed at each end of the column. A thin bottom layer of glass beads was used to maintain the bed followed by a glass wool layer to ensure separation of the glass beads and the adsorbent layers. A thick glass beads layer (2 cm) is set at the top of the adsorbent (2.5 cm) to ensure good stacking of the adsorbent and avoid channeling of influent solution during the adsorption process.

The influent solution is pumped into the column at a flowrate of 1.6 mL/min using a peristaltic pump (Ismatec Ecoline VC-MS/CA8-6). At first, the column is primed with distilled water to remove any excess air. Then the sorbate solution is passed into the column and the samples of the effluent solution are collected at specific periods of time. The samples are taken to the AAS to obtain the amount of each metal.

## G. Fixed-bed column adsorption modeling

The breakthrough curve is obtained using experimental data by plotting  $C_{out}/C_{in}$  as a function of time. Mathematical models were developed to analyze the breakthrough behavior in the fixed-bed adsorber.

- Thomas model

The Thomas model states that the adsorption is immediate. It is based on the assumption that the adsorption undergoes the pseudo-second order rate of kinetics, stating that the electrostatic interactions and axial dispersion may be negligible [54]. It is described by the following eq. (13):

$$\ln\left(\frac{C_{in}}{C_{out}} - 1\right) = \frac{k_T q_{max} m}{v} - k_T C_{in} t \quad (13)$$

$k_T$  is the Thomas rate constant (L/min·mg),  $q_{max}$  is the maximum adsorption concentration in the solid phase (mg/L),  $m$  is the mass of adsorbent used and  $v$  is the volumetric flow rate (L/min).

- Clark model

The Clark model was developed to study the performance of adsorption using the following eq. (14) [55]:

$$\ln\left[\left(\frac{C_{in}}{C_{out}}\right)^{n-1} - 1\right] = -rt + \ln B \quad (14)$$

where  $n$  is the Freundlich constant,  $r$  and  $B$  are the Clark model parameters. This model assumes that the Freundlich isotherm applies and that the adsorption rate is limited by the outer mass transfer step.

## CHAPTER III

### RESULTS AND DISCUSSION

#### **A. Characterization of SMCB and CB**

The properties of SMCB and CB and proximate analysis of non-carbonized materials are presented in Table 3. The SMCB surface area is  $9.22 \text{ m}^2/\text{g}$  while CB had a significantly higher surface area of  $34.3 \text{ m}^2/\text{g}$ . The moisture content of the raw material before carbonization is relatively high (45.8 and 36.2wt.% for SMCB and CB, respectively) as is the majority of bio-wastes. The char does not contain water directly after carbonization. The fixed carbon increased after carbonization from 8.9wt.% to 21.2wt.% FOR SMCB (calculated on a dry basis) and is relatively low, due to the high ash content that increased from 16.4wt.% to 50.6wt.% after treatment at high temperature. However, the volatile matter decreased significantly from 71.4wt.% to 13.8wt.%. In contrast, CB had different results as the ash content is lower than SMCB before and after carbonisation (3.7 and 38.2wt.%, respectively). The volatile matter and the fixed carbon are shown to be higher than SMCB as the volatile matter is 81.1wt.% before carbonisation and 18.9wt.% after it for CB and the fixed carbon is 11wt.% before carbonisation and 33.6wt.% after it. The higher heating value for SMCB is 13.8 MJ/kg and for CB 23.5 MJ/kg. It has been shown in previous studies that the heating value of biochars range from 12 to 44 MJ/kg, while the heating value of coal and charcoal is the range of 14 to 35 MJ/kg [56]. Carbonisation is an important process during which energy densification takes place: low-energy components are volatized and high-energy

components remain within the product obtained [57] suggesting that biochars have a potential for replacement of solid fossil fuels for clean energy production.

The surface functional groups were analyzed using FTIR, as shown in Figures 1 and 2. The SMCB showed three strong peaks: one at  $1100\text{ cm}^{-1}$  corresponding to an aliphatic ether C-O stretching vibration, and the other peaks at  $1424\text{ cm}^{-1}$ , and at  $877\text{ cm}^{-1}$  indicating the presence of the carbonate stretching and bending vibrations respectively of gypsum [58]. In addition, peaks,  $1566\text{ cm}^{-1}$  and  $1722\text{ cm}^{-1}$  indicate stretching vibrations of nitro N-O and aliphatic C=O, respectively. The chemical interactions between the biochar and its environment are related to the surface chemistry of the biochar. Thus, the presence of oxygenated functional groups suggests that adsorption may involve interactions with the functional groups present on the surface of SMCB. For the adsorption of the metal ions, the peak at  $750\text{ cm}^{-1}$  visible on SMCB before adsorption is less visible after the sorption. This is because most of the binding sites were used by metal ions for coordination. As the C-H stretching was affected, the M-C bond could be a metal-methylidyne (MCH), metal-methylidene ( $\text{MCH}_2$ ) or methyl-metal ( $\text{MCH}_3$ ) bond depending upon the ligand attached to the carbon atom [59]. After adsorption the peak at  $1100\text{ cm}^{-1}$  undergoes a shift to lower wavenumber ( $1020\text{ cm}^{-1}$ ) due to adsorption of the metal and weakening of the C-O bond [60]. At  $3300\text{ cm}^{-1}$  in case of Pb(II) adsorption the O-H alcohol peak disappeared after the Pb(II) adsorption, which will be later show the strongest sorption effect demonstrating that chemical interactions took place between the heavy metal cations and the surface functional groups of SMCB during adsorption.



The results for FTIR spectra of CB are shown in Figure 2. The functional groups present on the surface of CB before adsorption include a strong bending C=C bond at  $706\text{ cm}^{-1}$ . This bond was weakened after the adsorption of the three heavy metals. A bending -OH group is present at  $1398\text{ cm}^{-1}$ . This peak disappeared after the adsorption of Cu and Zn while it remained, but weakened, for Pb. This heavy metal will later be shown to have the strongest sorption effect. A strong stretching nitro compound N-O group at  $1547\text{ cm}^{-1}$  is observed. After the adsorption of the three metal ions, this peak was not as significantly strong, which shows a weakened N-O bond after adsorption. A peak at  $1100\text{ cm}^{-1}$  corresponds to an aliphatic ether C-O stretching vibration on CB before adsorption. As shown for SMCB, this peak is shifted to  $1020\text{ cm}^{-1}$  showing a weakening of the C-O bond. These results prove that the surface functionality of CB was modified and that chemical interactions took place during adsorption.

Table 3: Selected properties of spent mushroom compost and coconut shell (raw material) and elemental analyses of SMCB and CB

Parameters	Spent mushroom compost	Coconut shell	SMCB	CB
Moisture content, wt. %	45.8	36.2		
Ash content, wt. % d.b.	16.4	3.70	50.6	38.2
Volatile matter, wt. % d.b.	71.4	81.1	13.8	18.9
Fixed carbon, wt. % d.b.	8.9	11.0	21.2	33.6
Surface area, m <sup>2</sup> ·g <sup>-1</sup>			9.22	34.3
Higher heating value, MJ·kg <sup>-1</sup>			13.8	23.5
CEC, mmol·kg <sup>-1</sup>			57.6	63.0
C, wt. % d.b.			35.94	61.8
H, wt. % d.b.			1.21	1.75
N, wt. % d.b.			2.18	1.23
H/C molar ratio			0.03	0.03
Al, mg·kg <sup>-1</sup> d.b.			11.42	0.02
Ba, mg·kg <sup>-1</sup> d.b.			0.12	0.02
Ca, mg·kg <sup>-1</sup> d.b.			14.18	12.3
Cd, mg·kg <sup>-1</sup> d.b.			0.00	0.00
Co, mg·kg <sup>-1</sup> d.b.			0.00	0.00
Cr, mg·kg <sup>-1</sup> d.b.			0.00	0.01
Cu, mg·kg <sup>-1</sup> d.b.			0.36	0.10
Fe, mg·kg <sup>-1</sup> d.b.			2.14	0.43
K, mg·kg <sup>-1</sup> d.b.			33.76	12.9
Mg, mg·kg <sup>-1</sup> d.b.			5.45	1.93
Mn, mg·kg <sup>-1</sup> d.b.			0.72	0.22
Na, mg·kg <sup>-1</sup> d.b.			24.81	3.78
Ni, mg·kg <sup>-1</sup> d.b.			0.02	0.01
Pb, mg·kg <sup>-1</sup> d.b.			0.04	0.01
Zn, mg·kg <sup>-1</sup> d.b.			0.63	0.43

Hg, mg·kg <sup>-1</sup> <sub>d.b</sub>	0.01	0.01
P, mg·kg <sup>-1</sup> <sub>d.b</sub>	12.27	20.01
S, mg·kg <sup>-1</sup> <sub>d.b</sub>	48.12	3.86
Sb, mg·kg <sup>-1</sup> <sub>d.b</sub>	0.00	0.00
Se, mg·kg <sup>-1</sup> <sub>d.b</sub>	0.00	0.00

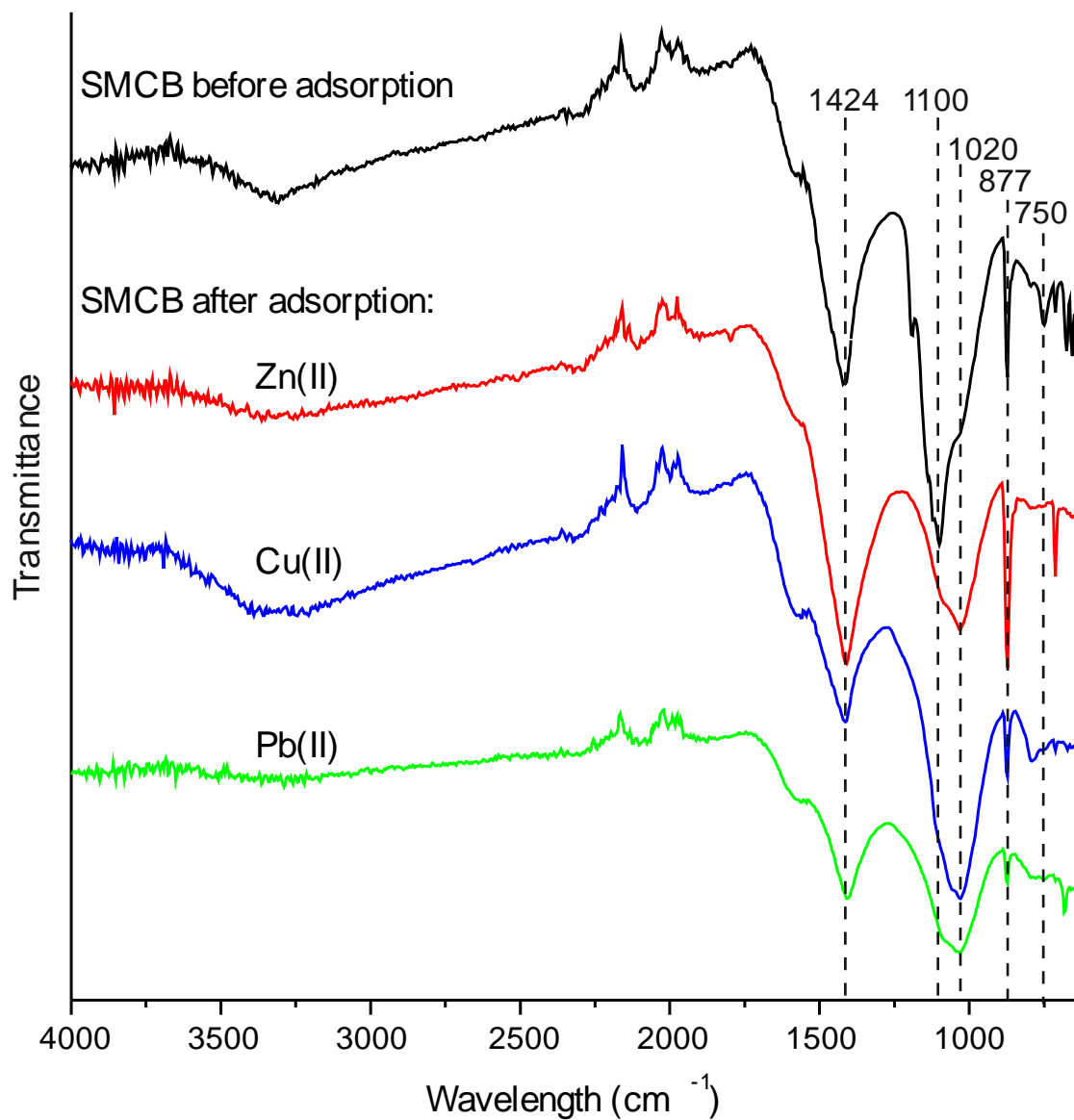


Figure 1: FTIR spectra of SMCB before adsorption, and after adsorption of Zn, Cu and Pb.

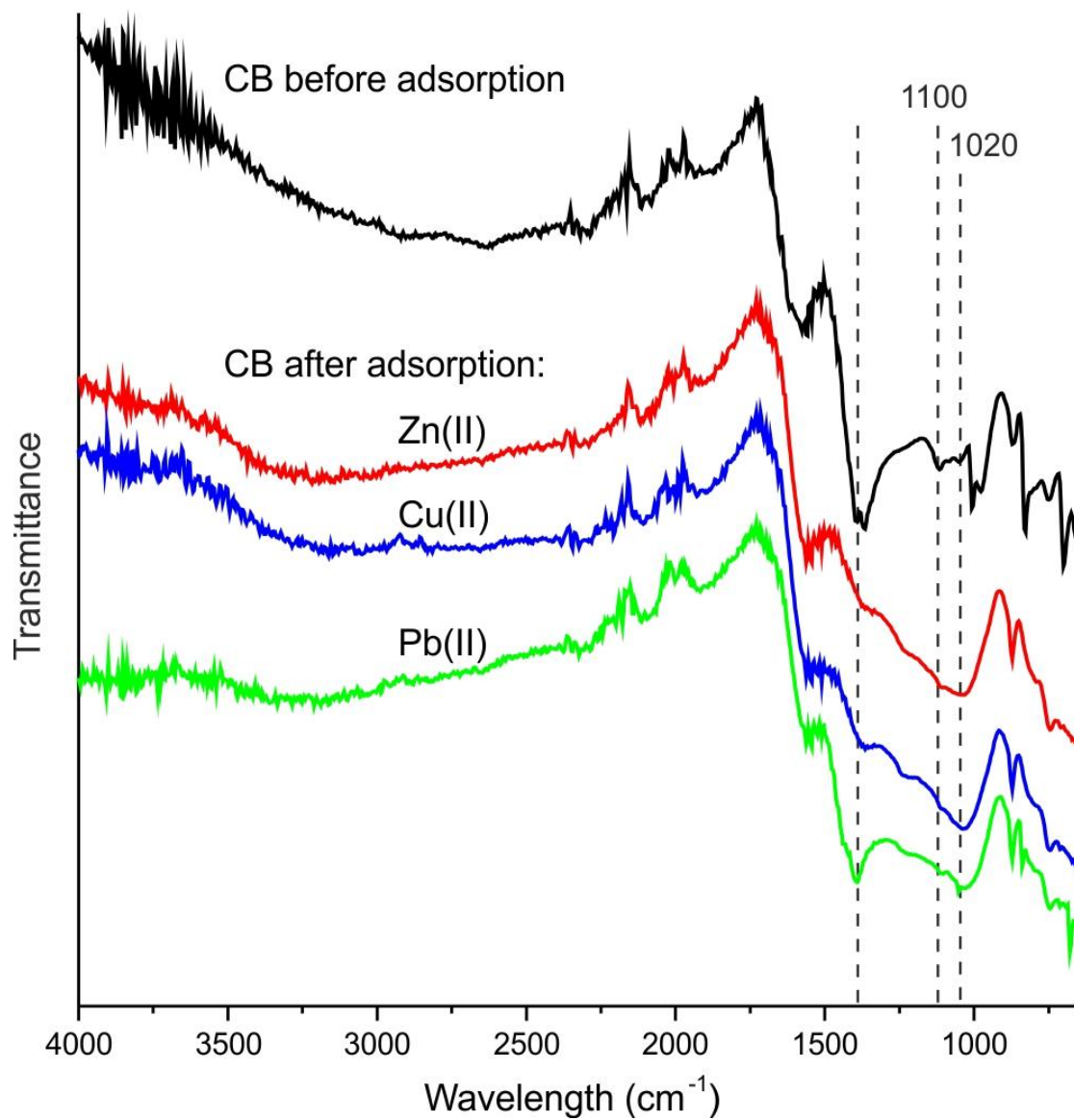


Figure 2: FTIR spectra of CB before adsorption, and after adsorption of Zn, Cu and Pb.

## **B. Cation Exchange Capacity**

The cation exchange capacity (CEC) is the amount of negative charge present within the biochar that attracts exchangeable cations, such as  $\text{Na}^+$ ,  $\text{Ca}^{2+}$ ,  $\text{K}^+$ ,  $\text{Fe}^{2+}$ ,  $\text{NH}_4^+$ ,  $\text{Mg}^{2+}$ , etc. Biochars have a specific metal binding capacity mainly due to the presence of hydroxyl, phenolic, carboxylate and carbonyl groups. Therefore, biochars that contain more hydrophilic and oxygen groups possess higher cation-exchanging ability and a higher nutrient retention capacity. CEC is expressed in moles of cations per kg of biochar. Based on the pH of the adsorption process, these groups can bind cations with different affinities, depending on the ion exchange properties of the biochar [61].

Digestion of the biochar was undertaken before and after adsorption of the heavy metals. This can help determine the concentration of cations present in the biochar to evaluate the amount lost from SMCB and CB after adsorption. A higher cation exchange will lead to a higher loss of metals from the biochar.

In addition, a CEC study was undertaken to investigate the involvement of the ion exchange mechanism in the adsorption process of the metal ions onto the biochars. The CEC was found to be moderate with a values of 57.6 and 63 mmol/kg for SMCB and CB, respectively. Biochars prepared from poultry litter and swine manure have a CEC of 70.3 and 91.4 mmol/kg, respectively, when carbonized at 400°C but it falls to 39.7 and 36.3 mmol/kg, respectively when carbonized at 600°C [62]. The results show that at higher pyrolysis temperature, the CEC decreases, showing that the ion exchange process becomes less important.

After carbonisation, the surface area of the biochars is modified and many functional groups are formed on the surface. The lower the carbonisation temperature, the more oxygenated functional groups produced, such as carboxylic and phenolic groups. These groups induce a greater nutrient retention capacity and a higher cation exchange. Hence, adsorption is determined by the chemical groups present on the biochar surface, and is known as chemisorption. However, when increasing the temperature, the C/O ratio increases and more aromatic compounds are formed. In this case, adsorption occurs mainly by electrostatic (cation- $\pi$ ) interaction and it is known as physisorption, which explains the lower CEC at higher carbonisation temperature [63-65]. In the case of SMCB and CB, chemisorption, including ion exchange, is involved in the adsorption of Zn(II), Cu(II) and Pb(II).

### C. Effect of initial pH

The initial pH of the solution has a significant effect on the adsorption process as it modifies the surface charge of the adsorbent. The experiments were conducted using the batch technique by adjusting the initial solution pH to 2, 4, 6, 8, 10 and 12. The change in pH after adsorption was calculated according to eq. (15):

$$\Delta\text{pH} = \text{pH}_e - \text{pH}_{\text{in}}, \quad (15)$$

with  $\text{pH}_e$  the value of pH at equilibrium, and  $\text{pH}_{\text{in}}$  the initial pH value.

$\Delta\text{pH}$  decreased with increasing initial pH value, as shown in Figures 3 and 4. The initial pH affects the surface charge of the biochar and the degree of precipitation of the metal ions in the solution. As the pH decreases, the biochar surface becomes more positively

charged and thus decreases the adsorption capacity of the positively charged metal ions. At low initial pH values for the adsorption onto SMCB, ranging from 2 to 4, the pH increased significantly (from 2 to 6.1 for Zn(II), 6.2 for Cu(II) and 7.5 for Pb(II)), which indicates the release of basic and carboxylic groups into solution resulting in the precipitation of heavy metals onto the biochars. Therefore, ion exchange and precipitation are involved in the adsorption process. Similar results were observed for the adsorption onto CB. As the initial pH increases, the change in pH decreases. At low pH values, a high amount of basic groups is released in solution, leading to an increase of pH from 2 to 9.42 and from 4 to 9.84 in the case of Zn and similarly for the other heavy metals. At low initial pH, the surface charge of the biochar is positive, which hinders the adsorption of the positively charged heavy metals. As the initial pH increases, the removal of heavy metal increases, showing that deprotonation takes place. When the pH is increased significantly (8 to 12), more basic groups are present in solution that lead to the hydrolysis of the metal ions and decrease their adsorption.

The point of zero charge ( $\text{pH}_{\text{pzc}}$ ) is the pH value at which the total charge of the internal and external surface of the biochar is zero. It is an important factor for the surface characterization of the sorbent [66]. This shows that basic and oxygenated functional groups are dominant on the biochar surface. In the case of SMCB, the  $\text{pH}_{\text{pzc}}$  is 9.91 for the adsorption of Zn(II), 8.40 for the adsorption of Cu(II) and 8.95 for the adsorption of Pb(II). In contrast, for CB, the  $\text{pH}_{\text{PZC}}$  is 10.02 for the adsorption of Zn(II), 9.58 for Cu(II) and 9.98 for Pb(II). It has been shown in the literature [66] that the  $\text{pH}_{\text{pzc}}$  value of biochars depends on carbonization temperature and conditions, and is in the region confirmed by this work.



The percentage removal of metal ions from solution by adsorption onto the biochars is presented in Figures 5 and 6. As the pH increases, more binding sites are liberated and leads to increased adsorption. Therefore, the optimum pH for adsorption to take place is  $\text{pH} = 6$  using both biochars, the value at which further adsorption experiments were conducted. The adsorption capacity onto SMCB at this pH value is 9.35 mg/g for Zn(II), 9.94 mg/g for Cu(II) and 51.26 mg/g for Pb(II). At higher pH values (pH 8 to 12) the metals ions are hydrolyzed and precipitation occurs, which hinders the adsorption of the metals. Similarly for the adsorption process onto CB, highest removal of heavy metals is observed at an initial pH of 6, as shown in Figure 5, the value at which all the following experiments are done. At a pH of 6, higher removal percent was observed for Zn using CB and for Cu using SMCB. Similar removal % was observed for Pb removal using both biochars. To further describe the adsorption process and the mechanisms involved during the adsorption process, the following experiments were performed.

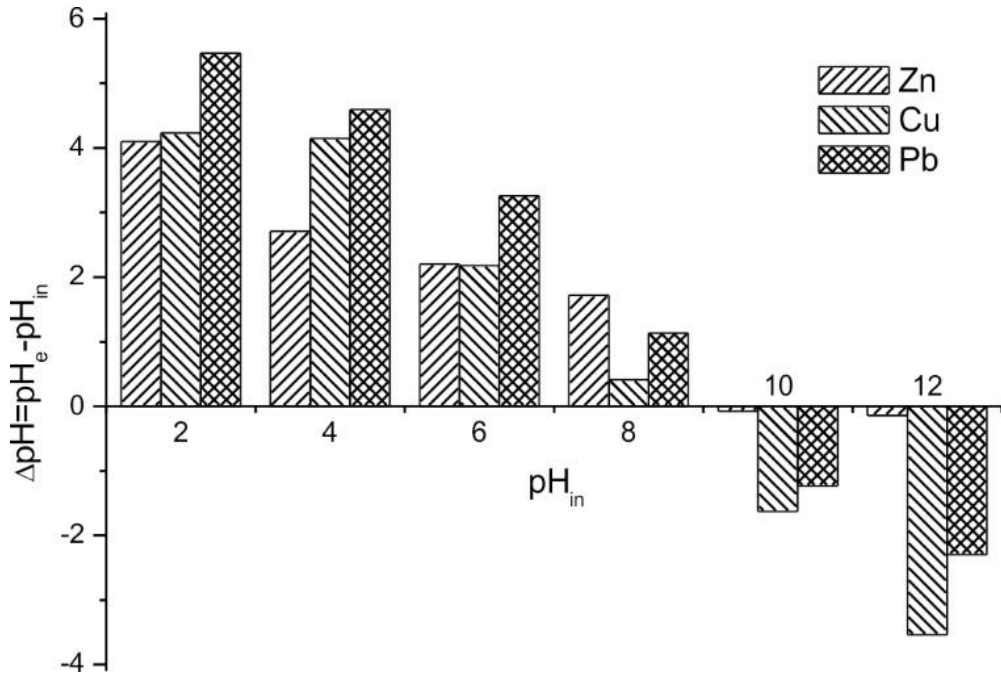


Figure 3: pH changes during metal ions adsorption on SMCB

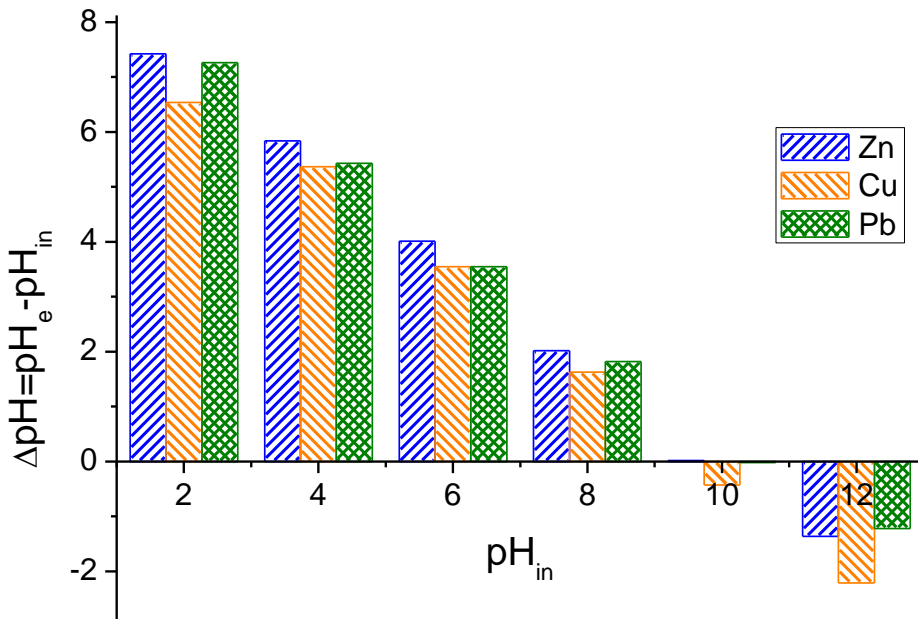


Figure 4: pH changes during metal ions adsorption on CB

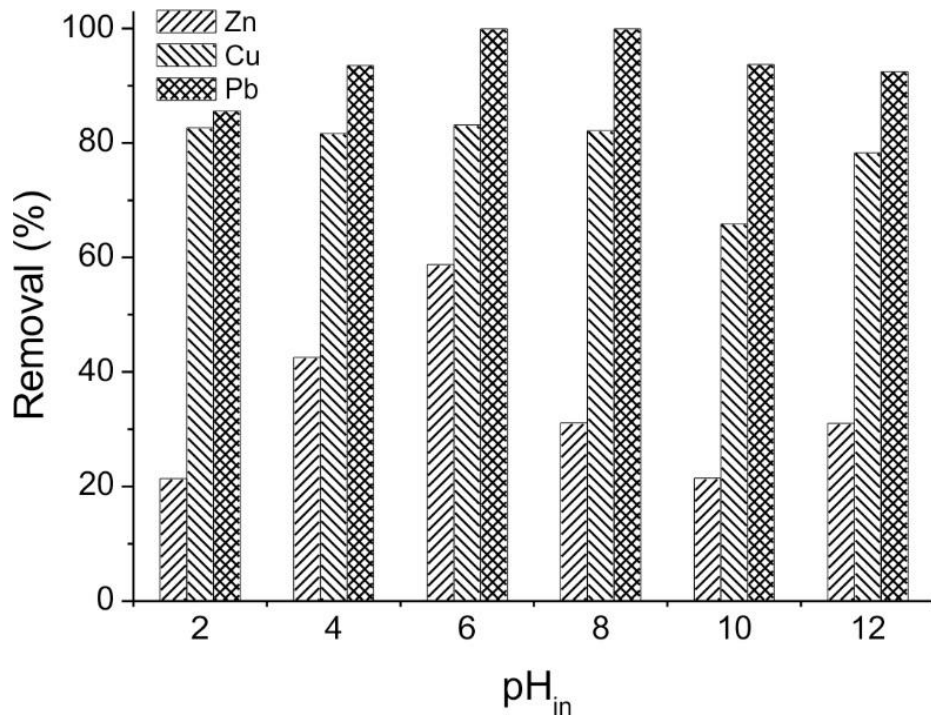


Figure 5: Percent of ions removal using SMCB as a function of initial pH

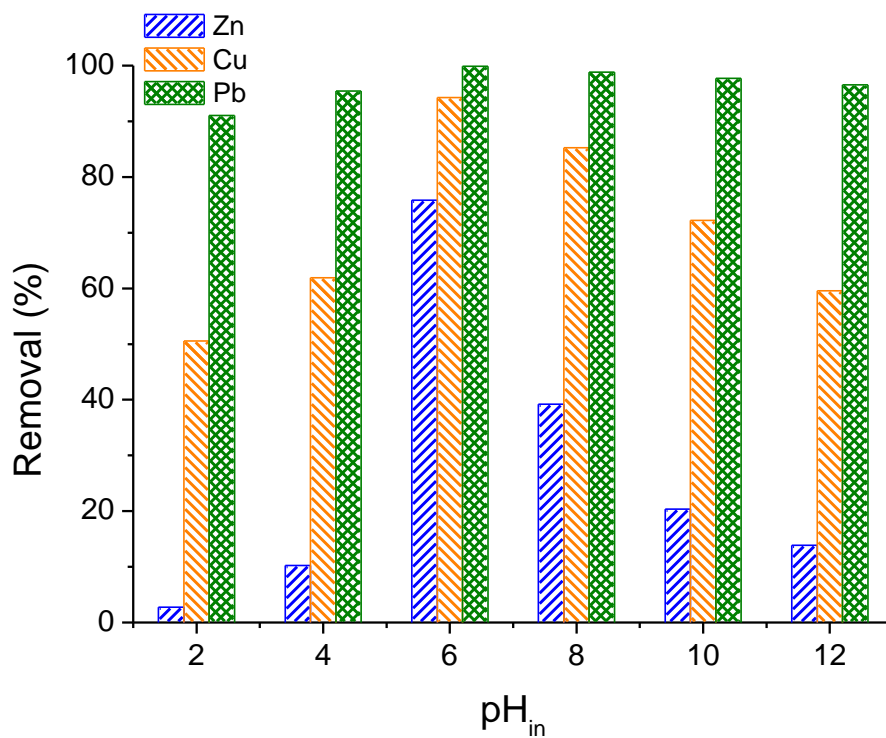


Figure 6: Percent of ions removal using CB as a function of initial pH

#### D. Adsorption isotherms

The adsorption equilibrium and its empirical models are significant for the application of biochars as adsorbents. They provide the basis to further understand the interaction between the adsorbent and the adsorbate, which is affected by the properties of the adsorbent used [50]. The adsorption data of the metal ions on SMBC samples were analysed using the Langmuir and Freundlich isotherm models. Figures 7 and 8 presents the isotherms along with the experimental data. As presented in Table 4, the best fitting model for the adsorption onto SMCB of Zn and Pb ions is the Langmuir isotherm (based on  $R^2$  values), showing that a monolayer adsorption takes place over energetically equivalent adsorption sites. The values of  $R_L$  are in the range of 0.004 to 0.190, proving that the adsorption process is favorable. As for the Cu ion, the best fit model is Freundlich with a higher  $R^2$  value than Langmuir. Thus, adsorption for this metal ion is likely to take place on a heterogeneous multilayer adsorption surface. The maximum adsorption ( $q_0$ ) is higher for Pb(II) than Cu(II) than Zn(II).

On the other hand, the Langmuir model describes the adsorption process onto CB most adequately due to a higher correlation coefficient  $R^2$ : 0.945 for Zn(II), 0.983 for Cu(II) and 0.989 for Pb(II) (Table 5). This suggests that a homogenous monolayer adsorption takes place on energetically equivalent adsorption sites on the surface of CB. Therefore, in general similar results for equilibrium isotherms were obtained for the adsorption of the heavy metals onto both biochars: CB and SMCB.

To confirm the Langmuir model and that a monolayer adsorption took place, equation (10) was used and it was found that after adsorption using CB the surface area is 8.4, 8.1 and 14.9  $m^2/g$  for Zn, Cu and Pb adsorption, respectively. The values are

similar to the biochar surface area (34.3 m<sup>2</sup>/g) to have a multilayer adsorption. Thus, we can conclude that a monolayer is formed and the Langmuir model describes the adsorption of the heavy metals onto CB. On the other hand, when SMCB was used, the surface area was found to be 6.1, 9.1 and 15.44 m<sup>2</sup>/g, which is similar also to the surface area of SMCB. Thus, a monolayer adsorption took place.

Table 4: Langmuir and Freundlich isotherm parameters for the adsorption of heavy metals ions onto SMCB

Metal ion	$q_{e, exp}$ mg·g <sup>-1</sup>	Langmuir				Freundlich		
		$q_0$ mg·g <sup>-1</sup>	$K_L$ L·mg <sup>-1</sup>	$R_L$ -	$R^2$ -	$K_F$ mg·g <sup>-1</sup>	$n$ -	$R^2$ -
Zn(II)	288.5	333.2	0.002	0.602	0.964	2.61	1.595	0.806
Cu(II)	383.5	364.2	0.012	0.190	0.912	23.75	2.561	0.950
Pb(II)	547.5	564.0	0.455	0.004	0.957	158.10	2.339	0.899

Table 5: Langmuir and Freundlich isotherm parameters for the adsorption of heavy metals ions onto CB

Metal ion	$q_{e, exp}$ mg·g <sup>-1</sup>	Langmuir				Freundlich		
		$q_0$ mg·g <sup>-1</sup>	$K_L$ L·mg <sup>-1</sup>	$R_L$ -	$R^2$ -	$K_F$ mg·g <sup>-1</sup>	$n$ -	$R^2$ -
Zn(II)	277.2	338.3	0.006	0.346	0.957	3.625	1.413	0.767
Cu(II)	257.6	315.9	0.005	0.384	0.985	4.652	1.602	0.943
Pb(II)	427.8	452.6	0.032	0.064	0.983	19.29	1.911	0.889

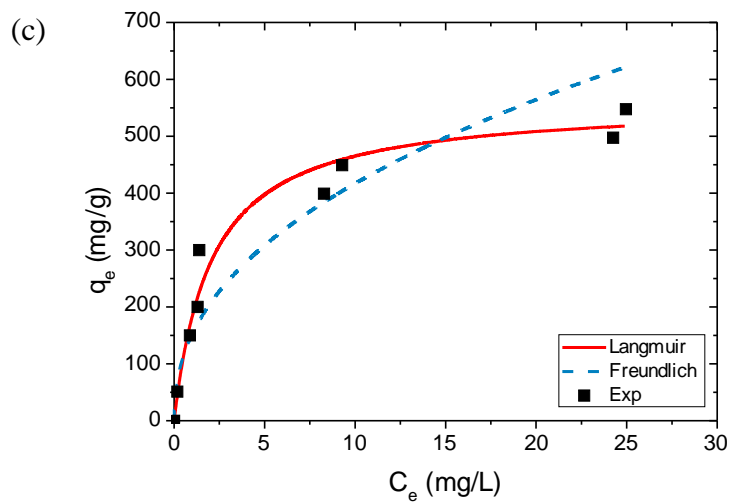
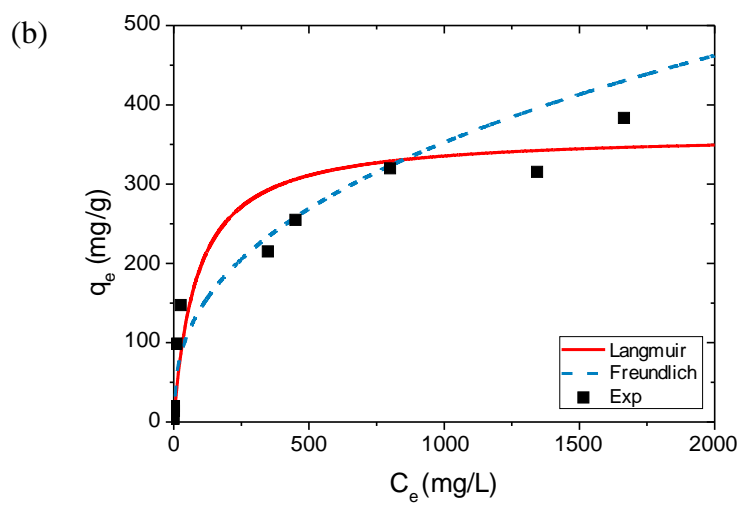
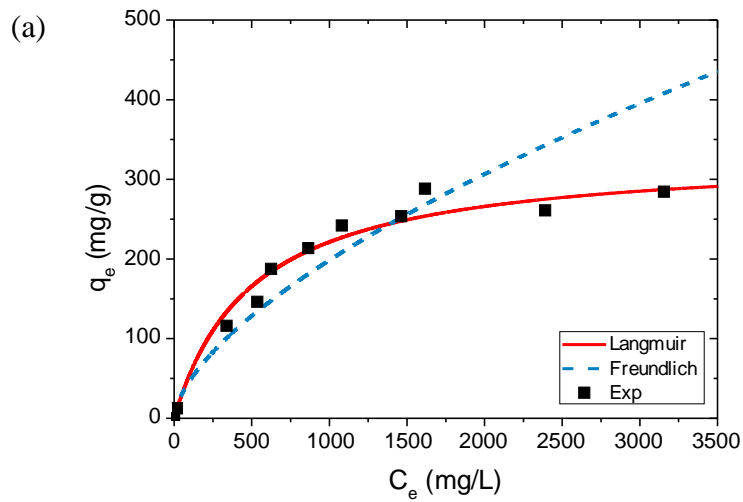
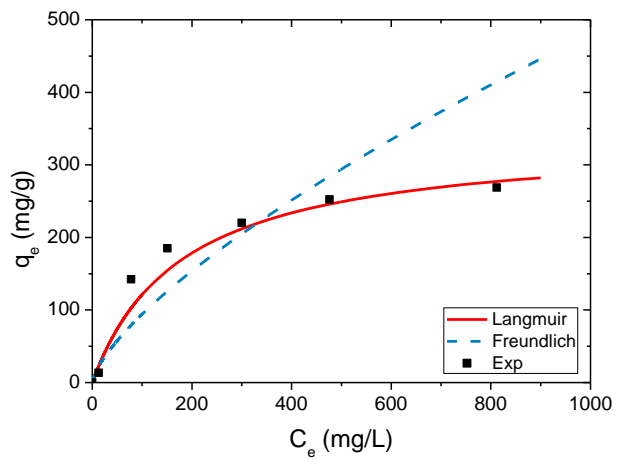
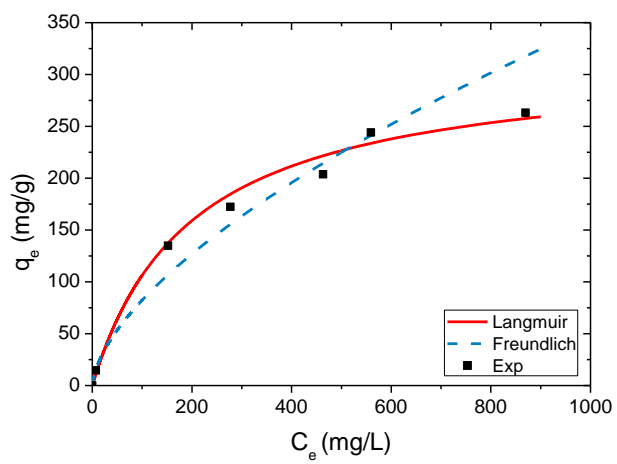


Figure 7: Adsorption isotherms of (a) Zn, (b) Cu and (c) Pb on SMCB

(a)



(b)



(c)

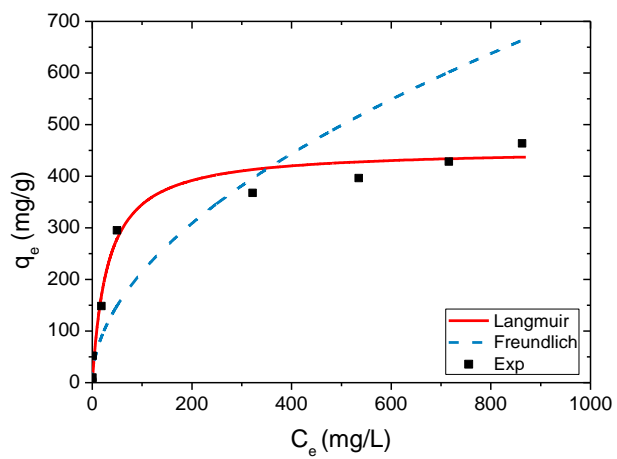


Figure 8: Adsorption isotherms of (a) Zn, (b) Cu and (c) Pb on CB

## E. Adsorption kinetics

The rate of adsorption and its dynamic behavior are important factors that must be investigated for the application of biochars to wastewater treatment. Biochars prepared from different feedstocks and at different carbonization conditions possess different structure and characteristics. The adsorption rate and capacity are a function of the properties of the biochar used, such as the aromaticity, porosity, surface area, polarity, etc [31]. Determination of the kinetic parameters can help assess the rate-limiting step and the contact time required for the adsorption process in adsorbents. Three of the most frequently used models were used to assess the rate-limiting step of adsorption: PFO, PSO and WM models. The resulting kinetic parameters are shown in Tables 6 and 7 with the best fitting model having the highest correlation factor ( $R^2$ ), between experimental and model data.

Figures 9 and 10 display the experimental data with PFO and PSO fitted models for the heavy metal adsorption onto SMCB at three different temperatures and CB at room temperature (20°C), respectively. The plots show a rapid increase in the adsorption capacity at the initial stage of adsorption, followed by a plateau which signals the onset of equilibrium. At the start of the adsorption process, a higher adsorption rate is observed due to more available adsorption sites. As adsorption proceeds, a lower increase in adsorption capacity is observed due to fewer available adsorption sites, until equilibrium is reached. Figure 9a shows that as the temperature is increased from 20°C to 60°C, a significant increase in the adsorption capacity of Zn(II) is observed. The  $R^2$  values are higher for PSO than PFO for every metal ions investigated. This shows that chemisorption, inner-sphere complexation and



precipitation may be involved during adsorption of these heavy metals ions onto SMCB. For Cu(II) and Pb(II). Figures 9 (b-c) show a less significant increase in the adsorption capacity than for Zn(II) as the temperature is increased for the other two ions. The  $R^2$  values obtained for Cu(II) are similar for PFO and PSO models. In addition, the values of  $h$  were shown to be higher for Pb(II) than Cu(II) than Zn(II). This shows a higher driving force between SMCB and Pb(II) during the process. The adsorption capacity obtained from PSO  $q_2$  increased from 10.08 to 14.93 mg/g for Zn(II), 14.74 to 15.75 mg/g for Cu(II) and 58.86 to 59.01 mg/g for Pb(II), when increasing the temperature from 20°C to 60°C. Thus, higher temperatures of adsorption lead to a higher heavy metal removal from the aqueous solutions. For the Pb(II) ions adsorption the  $R^2$  values for PFO model are very poor as the process was very fast and determination of adsorption capacity not close to equilibrium was not possible. In this case after even a short time (few seconds) the adsorbent was almost saturated by Pb(II) ions, and kinetic constants should be determined earlier than saturation.

As for the adsorption onto CB, the values of  $q_2$  are significantly higher for Pb(II) than for Cu(II) and Zn(II), which indicates that Pb has the highest adsorption capacity (51.96 mg/g). The adsorption capacity of Cu was 12.86 mg/g, higher than that of Zn (12.39 mg/g). The adsorption capacity of each metal ion onto CB was plotted as a function of shaking time ( $t$  [min]) along with the fitted models (Figures 10a-c). The curves show a significant increase initially showing that higher adsorption capacity is observed, due to higher availability of adsorption sites. The increase is then followed by a plateau indicating that equilibrium was reached after few seconds for Pb(II), after approximately 30 minutes for Cu(II) and 120 minutes for Zn(II).

By comparison of the kinetics data for both biochars, we can see that a higher adsorption capacity was observed when SMCB was used for Cu and Pb since at 20°C,  $q_{e,exp}$  was shown to be 14.83 mg/g when SMCB was used, higher than 12.66 mg/g using CB. Similarly for Pb, the values of  $q_{e,exp}$  are shown to be 58.89 mg/g when SMCB was used, higher than 51.99 mg/g using CB. However,  $q_{e,exp}$  is 9.65 mg/g for the adsorption of Zn using SMCB, lower than 12.21 mg/g using CB. The similar results were obtained when comparing the parameter  $q_2$  for the PSO model between the two biochars. Thus, the biochars have different adsorption capacities depending on their affinity to the heavy metals present in solution.

Table 6: Kinetics parameters for the adsorption of heavy metals using SMCB at different temperatures

Metal ion	T (°C)	$q_{e, exp}$ (mg·g <sup>-1</sup> )	Pseudo-first order model			Pseudo-second order model				Weber-Morris model		
			$q_1$ (mg·g <sup>-1</sup> )	$k_1$ (L·min <sup>-1</sup> )	$R^2$	$q_2$ (mg·g <sup>-1</sup> )	$k_2$ (g·mg <sup>-1</sup> ·min <sup>-1</sup> )	$h$ (mg·g <sup>-1</sup> ·min <sup>-1</sup> )	$R^2$	$k_i$ (mg·g <sup>-1</sup> ·min <sup>-0.5</sup> )	$\beta$	$R^2$
Zn(II)	20	9.65	9.72	0.013	0.950	10.08	0.003	0.29	0.969	0.701	0.22	0.971
	40	13.9	14.00	0.011	0.939	14.01	0.002	0.40	0.970	1.138	-0.56	0.919
	60	14.7	16.30	0.050	0.967	14.93	0.016	3.57	0.962	2.138	1.25	0.711
Cu(II)	20	14.83	14.84	0.184	0.939	15.09	0.021	4.86	0.972	2.722	2.32	0.984
	40	15.10	15.08	0.462	0.883	15.56	0.027	6.60	0.978	3.070	2.62	0.992
	60	15.21	15.22	0.607	0.941	15.75	0.051	12.58	0.987	3.589	2.10	0.979
Pb(II)	20	58.89	58.65	0.613	0.602	58.86	0.576	1997	0.999			
	40	59.03	58.94	0.158	0.336	58.91	1.699	5896	0.999			
	60	59.62	59.02	0.137	0.315	59.01	0.932	3245	0.999			

Table 7: Kinetics parameters for the adsorption of heavy metals using CB

Metal ion	$q_{e, \text{exp}}$ $\text{mg}\cdot\text{g}^{-1}$	Pseudo-first order model			Pseudo-second order model				Weber-Morris model		
		$q_1$ $\text{mg}\cdot\text{g}^{-1}$	$k_1$ $\text{L}\cdot\text{min}^{-1}$	$R^2$	$q_2$ $\text{mg}\cdot\text{g}^{-1}$	$k_2$ $\text{g}\cdot\text{mg}^{-1}\cdot\text{min}^{-1}$	$h$ $\text{mg}\cdot\text{g}^{-1}\cdot\text{min}^{-1}$	$R^2$	$k_i$ $\text{mg}\cdot\text{g}^{-1}\cdot\text{min}^{-0.5}$	$\beta$	$R^2$
Zn(II)	12.21	1.950	0.032	0.633	12.39	0.028	4.30	0.897	1.134	5.458	0.955
Cu(II)	12.66	3.212	0.239	0.950	12.86	0.024	4.01	0.955	2.901	0.474	0.904
Pb(II)	51.99	2.783	0.718	0.627	51.96	0.739	1994	0.999			

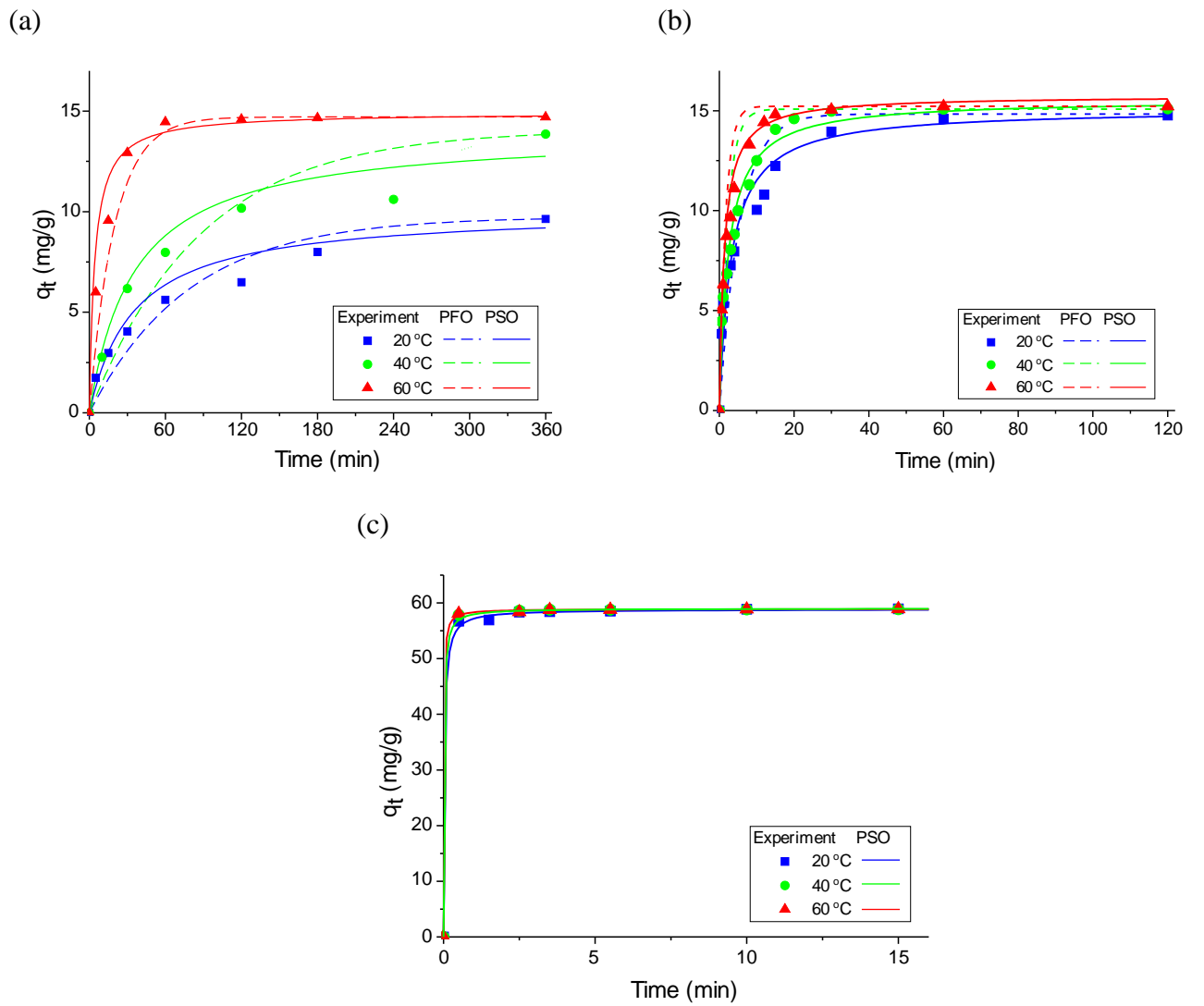
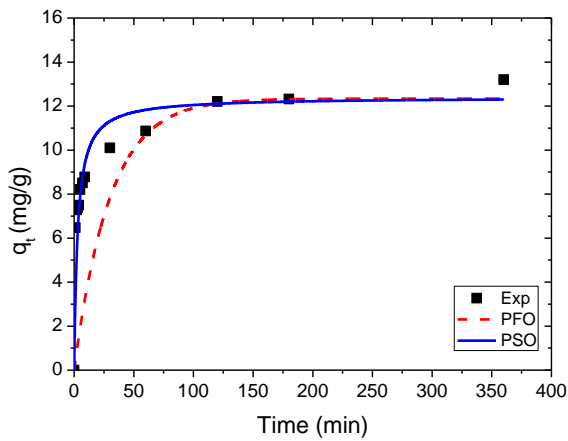
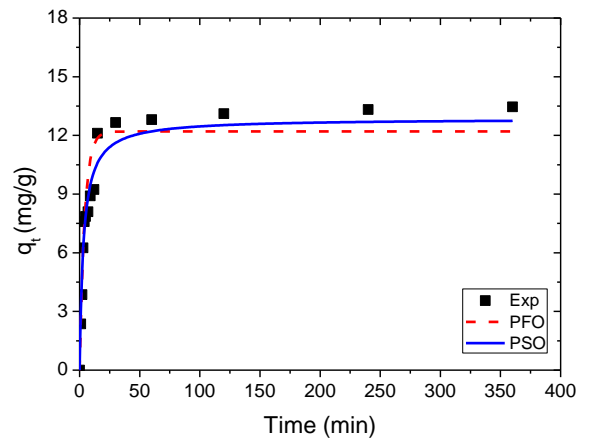


Figure 9: Kinetics for heavy metals ions (a) Zn, (b) Cu and (c) Pb adsorption on SMCB at various temperatures, experimental data described by pseudo-first order (PFO) and pseudo-second order (PSO).

(a)



(b)



(c)

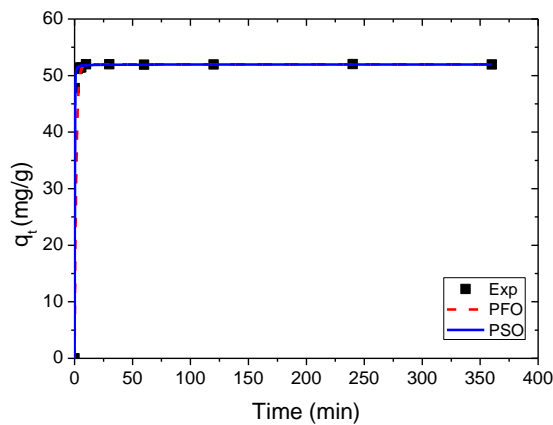


Figure 10: Kinetics for heavy metals ions (a) Zn, (b) Cu and (c) Pb adsorption on CB for the experimental data described by pseudo-first order (PFO) and pseudo-second order (PSO).

The WB model was studied to assess if intra-particle diffusion is the rate limiting step during the overall adsorption process. The parameters of the WM models are shown in Tables 6 and 7 for each biochar used. The constant  $\beta$  accounts for the boundary layer thickness during adsorption. The lower this value is, the lower the boundary effect will be. If  $\beta$  value is equal to zero, intra-particle diffusion is the only rate-limiting step. For the adsorption of Cu(II) and Zn(II) using SMCB, Figures 11 (a-b) were plotted to show the adsorption capacity as a function of  $t^{1/2}$ . Two separate parts were obtained from this plot before the equilibrium stage is reached (the plateau part): film diffusion (1<sup>st</sup> stage, dotted line) and to the intra-particle diffusion (2<sup>nd</sup> stage, solid line). The resulting straight lines do not pass through the origin for Zn(II), however the value of intercept ( $\beta$ ) ranges from -0.52 to 1.25 for temperatures 20°C to 60°C. This suggests that the boundary layer effect is negligible as the line representing the 2<sup>nd</sup> part (intra-particle diffusion) is almost crossing the origin. Thus, intra-particle diffusion plays a major role as a rate-limiting step during the adsorption of Zn(II). The straight lines do not pass through the origin for Cu(II), but they are close to the origin as the intercept ( $\beta$ ) values range from 2.10 to 2.62, showing that the boundary effect is not significant. Thus, intra-particle diffusion resistance affects the adsorption of Cu(II). The rate constant  $k_i$  was shown to increase with increasing temperature. For the Pb(II) adsorption using both biochars, the saturation was reached in a very short time and it was not possible to apply the WB model.

For the adsorption using CB, the adsorption capacity is obtained at 20°C and  $q_t$  is plotted as a function of  $t^{1/2}$  for Zn and Cu, as shown in Figure 12. For Zn, the line does not pass by the origin with a  $\beta$  value of 5.458. For Cu(II), the value of  $\beta$  is lower

(0.474), with the curve almost passing through the origin. In that case, intra-particle diffusion affects the Cu(II) adsorption more than the other heavy metal. Therefore, the intra-particle diffusion and boundary layer effects differs using different biochars for the adsorption of different heavy metals.

In most cases for earlier studies that the removal of heavy metals on biochars followed the PSO model [67]. Chen et al. (2011) [68] showed that the adsorption of Cu(II) and Zn(II) using hardwood and corn straw biochars follow a PSO model. Similar conclusions were made by Kolodynska et al. (2012) [31] for Cu(II), Zn(II), Cd(II) and Pb(II) on char made from various manures. Liu and Zhang [69] used pinewood and rice husk biochars for the adsorption of Pb(II), also followed a PSO model. In our study, the kinetics obtained results are in correlation with previous studies, indicating that surface reactions (chemisorption) play a significant role in the adsorption process.

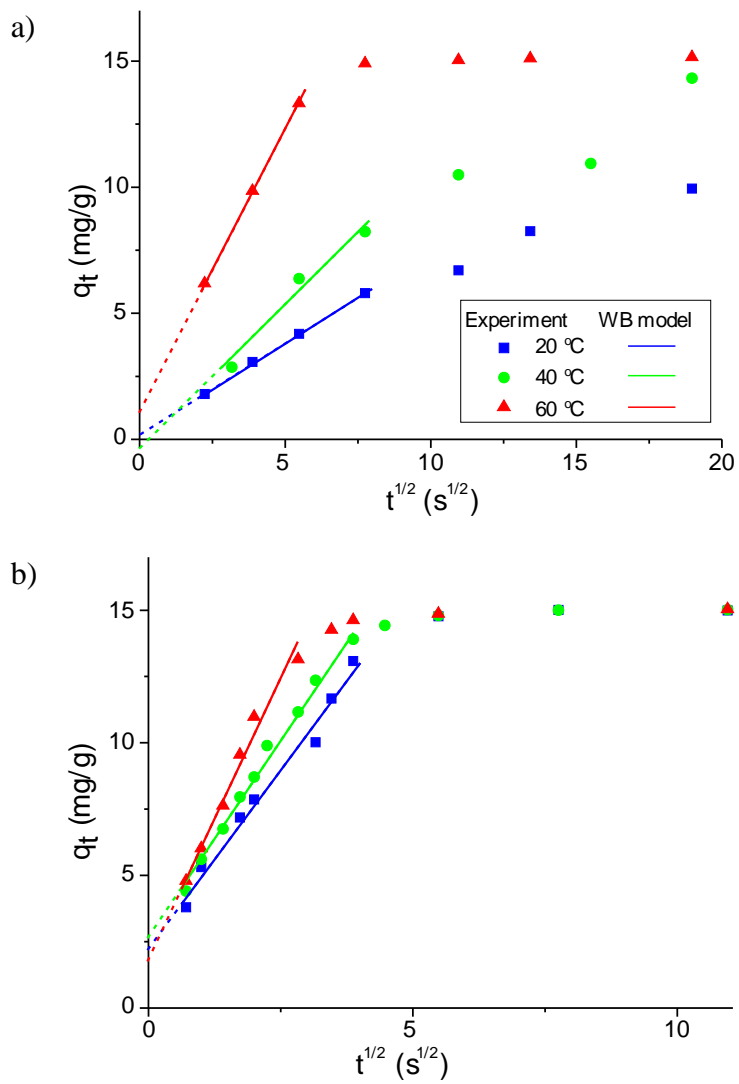


Figure 11: Kinetics for heavy metals ions (a) Zn and (b) Cu adsorption on SMCB at various temperatures, experimental data described by intra-particle diffusion Weber-Morris (WM) model.

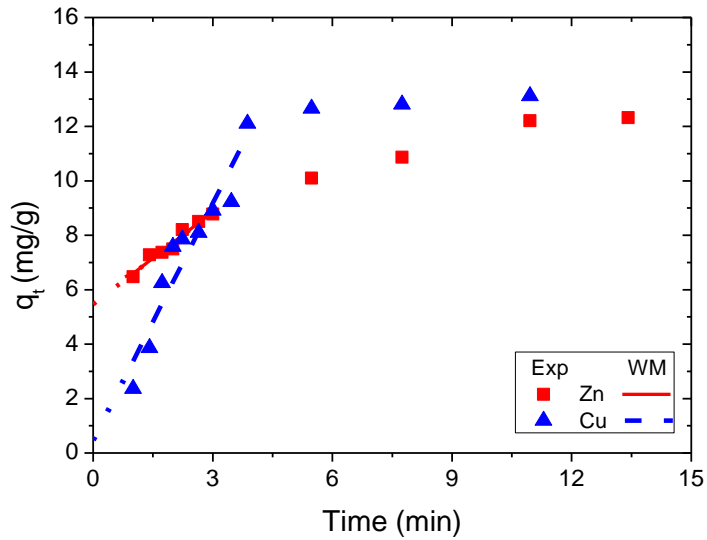


Figure 12: Kinetics for heavy metals ions Zn and Cu adsorption on CB with the experimental data described by intra-particle diffusion Weber-Morris (WM) model.

## F. Effect of temperature

The effect of temperature is an important physical parameter that must be studied to investigate its contribution on the change of adsorption capacity and efficiency [46]. The most significant adsorption capacity increase with temperature was observed for Zn (Figure 9-a). Thus, the adsorption was a temperature dependent process during which a higher and faster adsorption is observed when the temperature is increased. Thermodynamic parameters were obtained by varying the temperature to 20°C, 40°C and 60°C using the batch technique. The change in Gibbs free energy indicates the spontaneity and feasibility of the adsorption process. The enthalpy change shows if the process is exothermic or endothermic, while the entropy change can reflect the favorability of the adsorption. The results of these parameters are shown in Tables 7



and 8. For Zn(II) adsorption using SMCB,  $\Delta G^\circ$  value is positive at 20°C and becomes negative when the temperature is increased. This indicates that at room temperature, the adsorption process for Zn(II) is not spontaneous. As the temperature is increased, the adsorption process is facilitated and takes place spontaneously. For Pb(II) and Cu(II),  $\Delta G^\circ$  is negative, suggesting spontaneous removal using SMCB. Thus, Pb(II) and Cu(II) ions have a higher affinity to SMCB than Zn(II), which was also shown by a higher adsorption capacity (Table 8). In addition, the positive values of  $\Delta H^\circ$  and  $\Delta S^\circ$  prove that the adsorption process was endothermic and favorable with a good affinity between the metals and SMCB. When CB was used, similar results were obtained as a positive entropy is also observed with similar values. The same entropy change was obtained for Zn (27 kJ/mol). For Cu and Pb, a lower entropy change was observed using CB (0.21 and 0.08 kJ/mol, respectively). As for the enthalpy change, almost similar results were obtained for Zn (82.3 kJ/mol using SMCB and 79.2 kJ/mol using CB). The values differ for the adsorption of Cu and Pb. For Cu, the enthalpy change is of 125 kJ/mol using SMCB, higher than 61.6 kJ/mol using CB (Table 9). On the other hand, this value using SMCB for the adsorption of Pb (12.8 kJ/mol) is lower than the adsorption using CB (39.7 kJ/mol). The Gibbs free energy change for the adsorption using CB is negative for the adsorption of all three metal cations. As the temperature increased, the  $\Delta G^\circ$  value ranged from 0.14 to 11 kJ/mol for Zn(II), 0.07 to 8.49 kJ/mol for Cu(II) and 4.98 to 11.1 kJ/mol for Pb(II). Thus, the adsorption process using CB is spontaneous, endothermic, with good affinity of the biochar to the cations.

Table 8: The Gibbs free energy change for each metal ions at different temperatures, enthalpy and entropy changes using SMCB

Metal ion	Temperature	$\Delta G$	$\Delta H$	$\Delta S$
	$^{\circ}\text{C}$	kJ/mol	kJ/mol	kJ/mol
Zn(II)	20	3.73		
	40	-3.25	82.3	0.27
	60	-6.92		
Cu(II)	20	-4.20		
	40	-9.98	125	0.44
	60	-21.95		
Pb(II)	20	-10.39		
	40	-12.31	12.8	0.08
	60	-13.55		

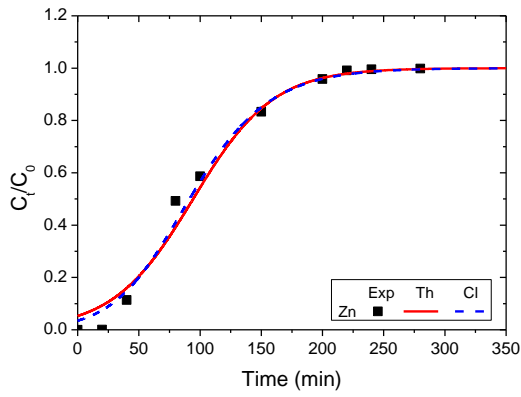
Table 9: The Gibbs free energy change for each metal ions at different temperatures, enthalpy and entropy changes using CB

Metal ion	Temperature	$\Delta G$	$\Delta H$	$\Delta S$
	$^{\circ}\text{C}$	kJ/mol	kJ/mol	kJ/mol
Zn(II)	20	-0.14		
	40	-4.09	79.2	0.27
	60	-11.0		
Cu(II)	20	-0.07		
	40	-4.01	61.6	0.21
	60	-8.49		
Pb(II)	20	-4.98		
	40	-6.78	39.7	0.15
	60	-11.1		

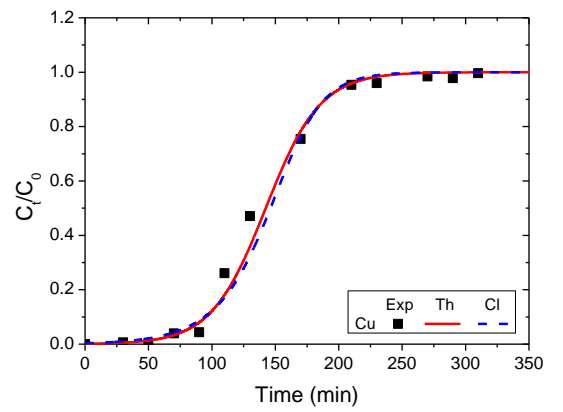
## G. Column adsorption modeling

The breakthrough curve was obtained for the different influent solutions used. It shows that the concentration of metals in the effluent increased with time. Adsorption models (Thomas and Clark models) are applied to the experimental data to assess the column adsorption parameters, as shown in Figure 13 (a-c) for SMCB and Figure 14 (a-b) for CB. The parameters obtained are shown in Tables 10 and 11. The Thomas model was used to determine the kinetic constant  $k_{Th}$  and the maximum concentration in the solid phase  $q_{max}$ . It assumes that the Langmuir model and pseudo-second order are applied. This assumption was confirmed by the previous kinetics and equilibrium experiments obtained by the batch experiments using both biochars. The results show that the highest  $q_{max}$  value was observed for Pb(II), which also confirms the results obtained in the batch experiments as Pb(II) had the highest adsorption capacity using CB and SMCB. In addition, Clark model was used and it assumes that the adsorption process follows the Freundlich isotherm, with a neglected axial dispersion in the column. Results show a high correlation factor for both models. From the breakthrough curves, the experimental data and the predicted values from the models show a negligible difference.

(a)



(b)



(c)

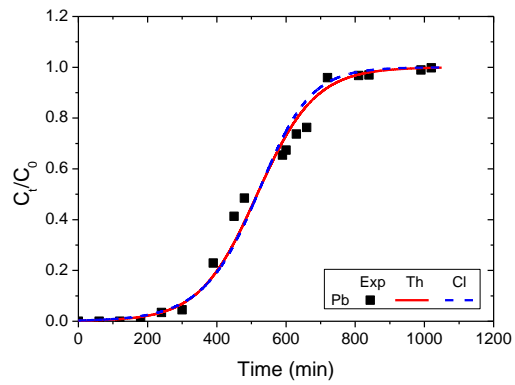
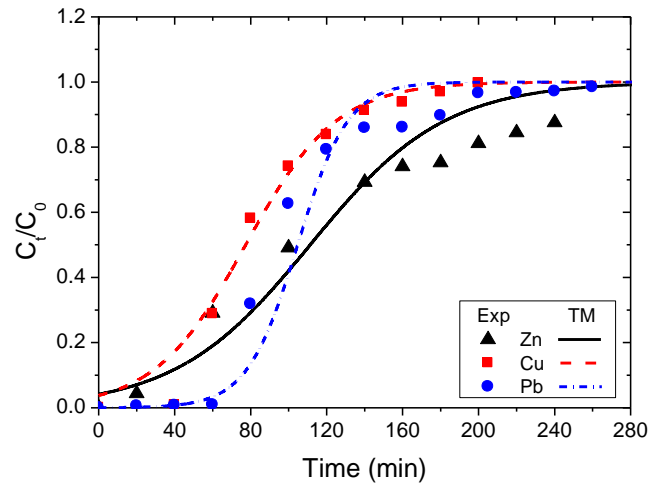


Figure 13. Experimental continuous adsorption  $C_t/C_0$  as a function of time in a single metal system for (a) Zn, (b) Cu and (c) Pb, described by the Thomas (Th) and Clark (Cl) models using SMCB

(a)



(b)

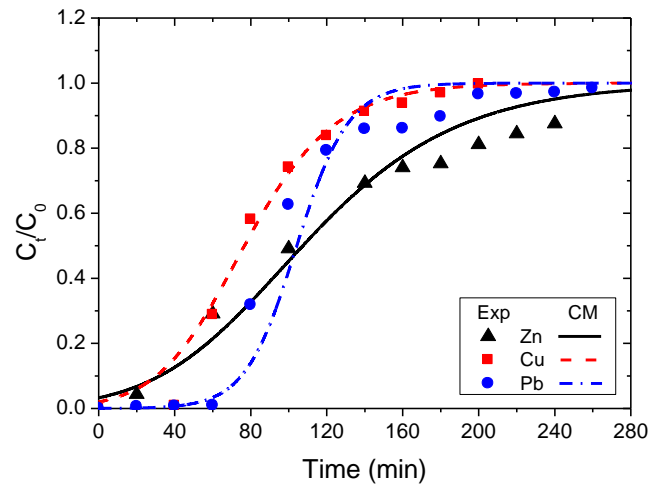


Figure 14. Experimental continuous adsorption  $C_t/C_0$  as a function of time in a single metal system for Zn, Cu and Pb, described by the (a) Thomas (TM) and (b) Clark (CM)

models

Table 10: Thomas and Clark model parameters for fixed-bed column using SMCB

Metal ion	Thomas model			Clark model		
	$k_{Th}$ ( $10^{-4}$ mL/min mg)	$q_{max}$ ( $10^4$ mg/g)	$R^2$ -	$A$ -	$r$ ( $\text{min}^{-1}$ )	$R^2$ -
Zn(II)	2.55	0.60	0.983	6.379	0.028	0.989
Cu(II)	3.19	1.11	0.991	6709	0.056	0.981
Pb(II)	0.26	12.7	0.985	2331	0.014	0.976

Table 11: Thomas and Clark model parameters for fixed-bed column using CB

Metal ion	Thomas model			Clark model		
	$k_{Th}$ ( $10^{-4}$ mL/min mg)	$q_{max}$ ( $10^4$ mg/g)	$R^2$ -	$A$ -	$r$ ( $\text{min}^{-1}$ )	$R^2$ -
Zn(II)	1.79	1.12	0.969	3.104	0.021	0.982
Cu(II)	2.74	0.76	0.979	9.437	0.038	0.983
Pb(II)	1.88	2.68	0.949	1556	0.072	0.953

## H. Competitive adsorption: batch and continuous systems

Often a competitive adsorption between the metals ions present in wastewater occurs. Thus, it is highly important to study the adsorption process of a multi-component system of heavy metals. Previous studies showed that the co-existence of several heavy metal cations in one system leads to a competition between the cations on the adsorption sites. Chen et al. demonstrated that competitive adsorption took place between Cu(II) and Zn(II) on biochar derived from hardwood and corn straw at metal concentrations higher than 1mM [70]. Ding et al. reported that the adsorption was more

favorable for Pb(II) than Cd(II) on biochar derived from water hyacinths [71]. In addition, Park et al. showed that a higher adsorption capacity was observed by Cu(II) than Cd(II) and Zn(II) on chicken bone-derived biochars [40]. In this study, the co-existence of the three heavy metals was studied in both batch and continuous systems. In the batch experiments, an increase in the concentration of the heavy metals lead to a decrease adsorption capacity of the cations. The effect of the mutual presence of  $\text{Pb}^{2+}$ ,  $\text{Cu}^{2+}$  and  $\text{Zn}^{2+}$  was evaluated with varying initial concentration, as shown in Tables 12 and 13. Using SMCB, the presence of Zn in a single system at a concentration of  $1 \cdot 10^{-3}$  mol/L showed an adsorption capacity of 6.431 mg/g. When adding Pb and Cu ( $1 \cdot 10^{-3}$  mol/L each), the adsorption capacity dropped to 4.238 mg/g. As the concentration of these metals was increased ( $3 \cdot 10^{-3}$  mol/L each), the adsorption capacity became even lower (1.878 mg/g). When increasing the initial concentration of Zn to  $3 \cdot 10^{-3}$  mol/L then to  $5 \cdot 10^{-3}$  mol/L, similar results were observed. The adsorption capacity of Zn at a concentration of  $5 \cdot 10^{-3}$  mol/L dropped from 20.41 to 2.59 mg/g after adding  $3 \cdot 10^{-3}$  mol/L of Cu and Pb. The adsorption capacity of Cu also decreased after increasing the amount of Pb and Zn. However, the decrease was less significant than in the case of Zn, as the adsorption capacity dropped from 6.347 to 6.046 mg/g (initial Cu concentration of  $1 \cdot 10^{-3}$  mol/L), 19.03 to 15.24 mg/g (initial Cu concentration of  $3 \cdot 10^{-3}$  mol/L) and 31.65 to 21.70 mg/g (initial Cu concentration of  $5 \cdot 10^{-3}$  mol/L). As for Pb, the adsorption capacity obtained is significantly higher than that for Cu and Zn in both the single and tertiary system, with a negligible decrease in the adsorption capacity when adding Cu and Zn. It was shown to be 20.71 mg/g, 62.14 mg/g and 103.5 mg/g at an initial concentration of  $1 \cdot 10^{-3}$  mol/L,  $3 \cdot 10^{-3}$  mol/L and  $5 \cdot 10^{-3}$  mol/L, respectively. Therefore,

the results show that the Pb metal ions have the highest affinity to SMCB compared to Cu and Zn during the adsorption process.

When CB was used, similar results were obtained. The adsorption capacity of Zn(II) decreased from 6.431 to 2.783 mg/g at an initial concentration of 1mM when increasing the concentration of Pb(II) and Cu(II) from 1 to 3 mM. Similar results were obtained when the initial concentration of Zn(II) was increased to 3 and 5 mM. Similarly for Cu(II), the adsorption capacity decreased when increasing the concentration of Pb(II) and Zn(II). At an initial Cu(II) concentration of 3mM, the adsorption capacity decreased from 18.77 to 16.23 mg/g when increasing the Pb(II) and Zn(II) initial concentration. As for Pb(II), similar results were obtained when increasing the concentration of the other two heavy metals. However, the adsorption capacity decrease is not as significant as for the other two metals. At an initial concentration of 5 mM, the adsorption capacity decreased from 32.11 to 17.26 mg/g for Zn(II) and 30.36 to 26.54 mg/g or Cu(II), while that of Pb(II) decreased from 102.9 to 101.7 mg/g. This proves that Pb(II) competes less than the other heavy metals on the adsorption sites as it has the highest affinity to the CB, similarly to when SMCB was used.



Table 12: Adsorption capacities of the heavy metals ions in a tertiary component system using SMCB

System	$q_e$ (mg/g)		
	Zn(II)	Cu(II)	Pb(II)
Zn (1mM)	6.431		
Zn (1mM) + Cu (1mM) + Pb (1mM)	4.238	6.291	20.60
Zn (1mM) + Cu (3mM) + Pb (3mM)	1.878	17.86	61.59
Zn (3mM)	17.80		
Zn (3mM) + Cu (1mM) + Pb (1mM)	7.744	6.226	20.41
Zn (3mM) + Cu (3mM) + Pb (3mM)	5.354	17.55	61.55
Zn (5mM)	20.41		
Zn (5mM) + Cu (1mM) + Pb (1mM)	5.690	6.164	20.28
Zn (5mM) + Cu (3mM) + Pb (3mM)	2.590	15.81	61.09
Cu (1mM)		6.347	
Cu (1mM) + Zn (1mM) + Pb (1mM)	5.248	6.264	20.63
Cu (1mM) + Zn (3mM) + Pb (3mM)	7.550	6.046	61.94
Cu (3mM)		19.03	
Cu (3mM) + Zn (1mM) + Pb (1mM)	3.708	17.58	20.30
Cu (3mM) + Zn (3mM) + Pb (3mM)	4.290	15.24	61.15
Cu (5mM)		31.65	
Cu (5mM) + Zn (1mM) + Pb (1mM)	2.118	27.09	19.80
Cu (5mM) + Zn (3mM) + Pb (3mM)	2.670	21.70	60.58
Pb (1mM)			20.71
Pb (1mM) + Zn (1mM) + Cu (1mM)	4.258	6.302	20.58
Pb (1mM) + Zn (3mM) + Cu (3mM)	10.21	18.61	20.51
Pb (3mM)			62.14
Pb (3mM) + Zn (1mM) + Cu (1mM)	3.728	6.293	62.01
Pb (3mM) + Zn (3mM) + Cu (3mM)	8.260	18.49	61.90
Pb (5mM)			103.5
Pb (5mM) + Zn (1mM) + Cu (1mM)	2.748	6.280	103.4
Pb (5mM) + Zn (3mM) + Cu (3mM)	5.370	17.49	102.9

Table 13: Adsorption capacities of the heavy metals ions in a tertiary component system using CB

System	q <sub>e</sub> (mg/g)		
	Zn(II)	Cu(II)	Pb(II)
Zn (1mM)	6.431		
Zn (1mM) + Cu (1mM) + Pb (1mM)	4.758	6.183	20.46
Zn (1mM) + Cu (3mM) + Pb (3mM)	2.783	18.40	61.26
Zn (3mM)	19.60		
Zn (3mM) + Cu (1mM) + Pb (1mM)	17.08	6.094	20.40
Zn (3mM) + Cu (3mM) + Pb (3mM)	10.11	13.15	60.89
Zn (5mM)	32.11		
Zn (5mM) + Cu (1mM) + Pb (1mM)	29.26	5.921	20.38
Zn (5mM) + Cu (3mM) + Pb (3mM)	17.26	11.87	59.96
Cu (1mM)		6.313	
Cu (1mM) + Zn (1mM) + Pb (1mM)	5.598	5.710	20.01
Cu (1mM) + Zn (3mM) + Pb (3mM)	18.32	5.156	61.94
Cu (3mM)		18.77	
Cu (3mM) + Zn (1mM) + Pb (1mM)	4.708	17.60	18.59
Cu (3mM) + Zn (3mM) + Pb (3mM)	16.17	16.23	60.60
Cu (5mM)		30.36	
Cu (5mM) + Zn (1mM) + Pb (1mM)	3.428	27.84	14.86
Cu (5mM) + Zn (3mM) + Pb (3mM)	14.04	26.54	50.16
Pb (1mM)			20.67
Pb (1mM) + Zn (1mM) + Cu (1mM)	4.748	5.739	20.51
Pb (1mM) + Zn (3mM) + Cu (3mM)	16.38	18.49	20.34
Pb (3mM)			61.90
Pb (3mM) + Zn (1mM) + Cu (1mM)	4.668	5.568	61.59
Pb (3mM) + Zn (3mM) + Cu (3mM)	16.04	18.02	61.18
Pb (5mM)			102.9
Pb (5mM) + Zn (1mM) + Cu (1mM)	4.168	3.759	102.2
Pb (5mM) + Zn (3mM) + Cu (3mM)	15.19	14.73	101.7

The competitive adsorption was also studied in the fixed-bed continuous column to assess to breakthrough curves of the metal cations when present in one system. The results show that Zn(II) is the first to leave the column in the effluent, followed by Cu(II) then Pb(II), as shown in Figures 15 and 16. Thus, when the metals are all present in the column, Zn ions have the least affinity to SMCB and CB as they do not adsorb and remain in the column as Cu and Pb ions. The breakthrough of the Cu ion takes place shortly after Zn(II), showing that it has a higher affinity than Zn(II), but lower than that of Pb(II). These results conform to the previous conclusions obtained from the batch studies using both biochars: CB and SMCB.

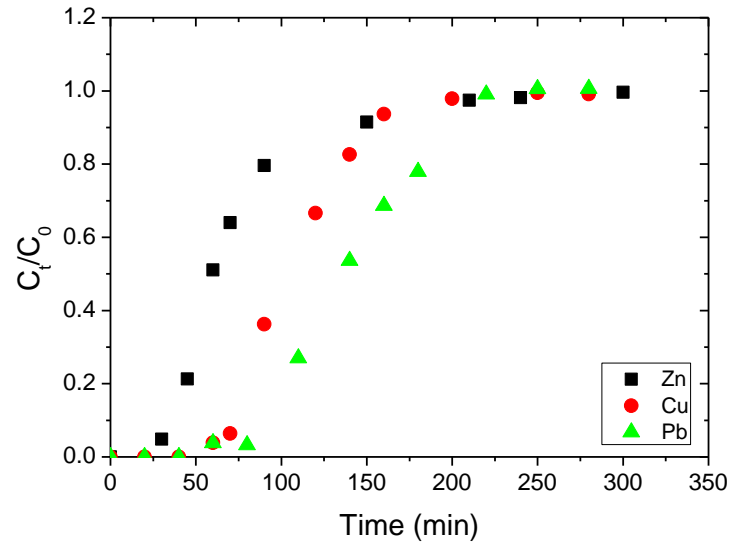


Figure 15. Experimental  $C_t/C_0$  as a function of time for Pb, Cu and Zn when mutually present in a tertiary system in a fixed-bed continuous adsorption using SMCB.

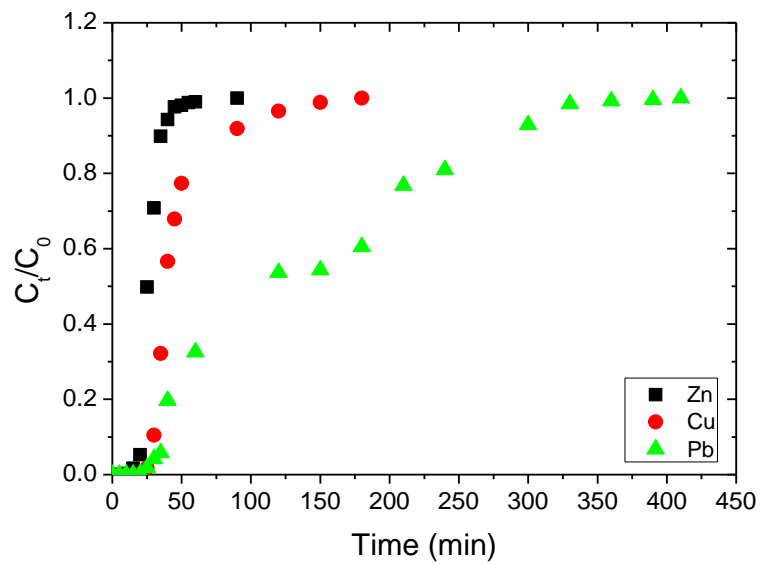


Figure 16. Experimental  $C_t/C_0$  as a function of time for Pb, Cu and Zn when mutually present in a tertiary system in a fixed-bed continuous adsorption using CB.

## CHAPTER IV

### CONCLUSION

SMCB and CB were shown to be excellent adsorbent for the removal of Pb(II), good for Cu(II) and moderate for Zn(II). The pH of the solution increased during adsorption showing a release of OH<sup>-</sup> ions and the oxygenated groups are lost from the surface of the biochar after adsorption. The biochars have a moderate value of CEC. The adsorption process was mainly conducted by chemisorption as the pseudo-second order model was the best fit. Intra-particle diffusion plays a major role as a rate-limiting step during the adsorption Zn ion using SMCB and Cu ion using CB. The best fitting equilibrium isotherm model is the Langmuir model, indicating that a monolayer homogenous adsorption took place on sorbent sites with equivalent energy for the metal ions. Thermodynamic parameters showed that the adsorption process is endothermic and favorable with good affinity between metals and the biochars. The results obtained by batch studies show that the biochars have similar removal capacities to the heavy metals. The adsorption capacity depends on the biochar used as well as its affinity to the specific sorbate in solution. At last, fixed-bed continuous adsorption was investigated for further application of SMCB and CB in heavy metal adsorption. The breakthrough curve was obtained for each heavy metal and the Thomas and Clark models were used to describe the breakthrough behavior. Competitive adsorption was performed in both batch and continuous systems to investigate the adsorption capacity for the mutual presence of the heavy metals. The data show that the highest affinity for SMCB and CB was with the Pb ions, which is in confirmation with the results obtained using the batch technique.

## BIBLIOGRAPHY

- [1] D. Mohan, C. U. Pittman, M. Bricka, F. Smith, B. Yancey, J. Mohammad, . . . H. Gong, Sorption of arsenic, cadmium, and lead by chars produced from fast pyrolysis of wood and bark during bio-oil production, *Journal of Colloid and Interface Science*, 310 (2007) 57-73.
- [2] B. Volesky, *Biosorption of heavy metals*, CRC press, 1990.
- [3] P.N. Gabby, *Lead: in mineral commodity summaries*. Reston, VA, U.S. Geological Survey, 2006.
- [4] S.J.S Flora, G. Saxena, P. Gautam, P. Kaur, K.D. Gill, Lead induced oxidative stress and alterations in biogenic amines in different rat brain regions and their response to combined administration of DMSA and MiADMSA, *Chem Biol Interac.* 170 (2007) 209–220.
- [5] D.B. Akers, M.F. Maccarthy, J.A. Cunningham, J. Annis, J.R. Mihelcic, Lead (Pb) contamination of self-supply groundwater systems in coastal madagascar and predictions of blood lead levels in exposed children, *Environmental Science & Technology*, 49 (2015) 2685-2693.
- [6] M.A. Momodu, C.A. Anyakora, Heavy metal contamination of ground water: the surulere case study, *Research Journal Environmental and Earth Sciences*, 2 (2010) 39-43.
- [7] Environmental Protection Agency, Chapter 4 - Geochemical assessment in historic mine sites - Inventory and Risk Classification. 60-74, 2009.

[https://www.epa.ie/pubs/reports/land/mines/CHAPTER4\\_Geochemical\\_%20Assessment.pdf](https://www.epa.ie/pubs/reports/land/mines/CHAPTER4_Geochemical_%20Assessment.pdf)

[8] A. Kabata-Pendias, A.B. Mukherjee, Trace elements from soil to human, Springer-Verlag, New York, 2007.

[9] M. Barakat, New trends in removing heavy metals from industrial wastewater, *Arabian Journal of Chemistry*, 4 (2011) 361-377.

[10] A. da Silva Oliveira, A. Bocio, T. M. B. Trevilato, A. M. M. Takayanagui, J. L. Domingo, S. I. Segura-Muñoz, Heavy metals in untreated/treated urban effluent and sludge from a biological wastewater treatment plant. *Environmental Science and Pollution Research-International*, 14 (2007), 483.

[11] N. Gupta, D. Khan, K. Santra, An Assessment of Heavy Metal Contamination in Vegetables Grown in Wastewater-Irrigated Areas of Titagarh, West Bengal, India. *Bulletin of Environmental Contamination and Toxicology*, 80 (2008), 115-118.

[12] W. Kwapinski, C. Byrne, E. Kryachko, P. Wolfram, C. Adley, J.J. Leahy, E.H. Novotny, M.H.B Hayes. Biochar from waste and biomass, *Waste and Biomass Valorization*, 1 (2010) 177–189.

[13] J. Lehmann, S. Joseph, Biochar for environmental management: science, technology and implementation, Routledge, 2015.

[14] S. Wang, B. Gao, A.R. Zimmerman, Y. Li, L. Ma, W.G. Harris, K.W. Migliaccio, Physicochemical and sorptive properties of biochars derived from woody and herbaceous biomass, *Chemosphere*, 134 (2015) 257–262.

- [15] Y. Han, A.A. Boateng, P.X. Qi, I.M. Lima, J. Chang, Heavy metal and phenol adsorptive properties of biochars from pyrolyzed switchgrass and woody biomass in correlation with surface properties, *J Environ Manag*, 118 (2013).
- [16] S. Yiacoumi, C. Tien, Adsorption of Metal Ions from Aqueous Solutions: Model Application, *Kinetics of Metal Ion Adsorption from Aqueous Solutions*, 1995, 151-201.
- [17] J Lehmann S. Joseph, *Biochar for Environmental Management: Science and Technology*. London; Sterling, VA: Earthscan 2009., editor. 2009.
- [18] R. R. Domingues, P. F. Trugilho, C. A. Silva, I. C. N. de Melo, L. C. Melo, Z. M. Magriotis, M. A. Sánchez-Monedero, Properties of biochar derived from wood and high-nutrient biomasses with the aim of agronomic and environmental benefits, *PloS one*, 12 (2017).
- [19] M. Kobya, E. Demirbas, E. Senturk, M. Ince, Adsorption of heavy metal ions from aqueous solutions by activated carbon prepared from apricot stone. *Bioresour. Technol.* 96 (2005), 1518–1521.
- [20] M. M. Johns, W. E. Marshall, C. A. Toles, Agricultural by-products as granular activated carbons for adsorbing dissolved metals and organics. *J. Chem. Technol. Biotechnol.* 71 (1998), 131–140.
- [21] R. R. Bansode, J. N. Losso, W. E. Marshall, R. M. Rao, R. J. Portier, Adsorption of metal ions by pecan shell-based granular activated carbons, *Bioresour. Technol.* 89 (2003), 115–119.



- [23] L. Agoubordea, R. Navia, Heavy metals retention capacity of a non- conventional sorbent developed from a mixture of industrial and agricultural wastes. *J. Hazard. Mater.* 167 (2009), 536–544.
- [23] B. Nasernejad, T. E. Zadeh, B. B. Pour, M. E. Bygi, A. Zamani, Comparison for biosorption modeling of heavy metals (Cr (III), Cu (II), Zn (II)) adsorption from wastewater by carrot residues, *Process Biochem.* 40 (2005), 1319–1322.
- [24] J. H. Park, Y. S. Ok, S. H. Kim, J. S. Cho, J. S. Heo, R. D. Delaune, D. C. Seo, Evaluation of phosphorus adsorption capacity of sesame straw biochar on aqueous solution: influence of activation methods and pyrolysis temperatures. *Environmental geochemistry and health*, 37 (2015), 969-983.
- [25] G. Chen, C. Peng, J. Fang, Y. Dong, X. Zhu, H. Cai, Biosorption of fluoride from drinking water using spent mushroom compost biochar coated with aluminum hydroxide, *Desalination and Water Treatment*, 57 (2015) 12385-12395.
- [26] F.J. Gea, M. Santos, F. Díaz, J.C. Tello, M.J. Navarro, Effect of spent mushroom compost tea on mycelial growth and yield of button mushroom (*Agaricus bisporus*), *World Journal Microbiological Biotechnology* 28 (2012) 2765–2769.
- [27] S.N. Jordan, G.J. Mullen, M.C. Murphy, Composition variability of spent mushroom compost in Ireland, *Biosource Technology*, 99 (2008) 411-418
- [28] S.N. Jordan, L.B. Holland, S.U. Linnane, Spent mushroom compost management and options for use, Environmental Protection Agency, Wexford, Ireland, 2012.
- [29] M. Lathika, C. A. Kumar, Growth trends in area, production and productivity of coconut in India. *Indian journal of agricultural economics*, 60 (2005).

- [30] P. H. Singh, Coconut industry in India-Challenges and opportunities. *INDIAN COCONUT JOURNAL-COCHIN-*, 29 (1998), 4-27.
- [31] D. Kołodzinska, J. Krukowska, P. Thomas, Comparison of sorption and desorption studies of heavy metal ions from biochar and commercial active carbon, *Chemical Engineering Journal*, 307 (2017) 353-363.
- [32] R. Han, Y. Wang, X. Zhao, Y. Wang, F. Xie, J. Cheng, Adsorption of methylene blue by phoenix tree leaf powder in a fixed-bed column: Experiments and prediction of breakthrough curves, *Desalination*, 245 (2009) 284–297.
- [33] M. S. Onyango, T. Y. Leswifi, A. Ochieng, D. Kuchar, F. O. Otieno, H. Matsuda, Breakthrough Analysis for Water Defluoridation Using Surface-Tailored Zeolite in a Fixed Bed Column, *Industrial & Engineering Chemistry Research*, 48 (2009), 931-937.
- [34] E. D. Freitas, H. J. Almeida, A. F. Neto, M. G. Vieira, Continuous adsorption of silver and copper by Verde-lodo bentonite in a fixed bed flow-through column, *Journal of Cleaner Production*, 171 (2018), 613-621.
- [35] G. M. Walker, L. R. Weatherley. Fixed bed adsorption of acid dyes onto activated carbon, *Environmental Pollution*, 99 (1998), 133-136.
- [36] S. Afroze, T. K. Sen, H. M. Ang, Adsorption performance of continuous fixed bed column for the removal of methylene blue (MB) dye using *Eucalyptus sheathiana* bark biomass, *Research on Chemical Intermediates*, 42 (2016), 2343-2364.
- [37] Biswas, Swarup, and Umesh Mishra. "Continuous fixed-bed column study and adsorption modeling: removal of lead ion from aqueous solution by charcoal originated

from chemical carbonization of rubber wood sawdust." *Journal of Chemistry* 2015 (2015).

[38] Z. Ding, X. Hu, Y. Wan, S. Wang, B. Gao, Removal of lead, copper, cadmium, zinc, and nickel from aqueous solutions by alkali-modified biochar: Batch and column tests. *Journal of Industrial and Engineering Chemistry*, 33 (2016), 239-245.

[39] S. Vilvanathan, S. Shanthakumar, Column adsorption studies on nickel and cobalt removal from aqueous solution using native and biochar form of *Tectona grandis*. *Environmental Progress & Sustainable Energy*, 36 (2017), 1030-1038.

[40] J. Park, J. Cho, Y. S. Ok, S. Kim, S. Kang, I. Choi, . . . D. Seo, Competitive adsorption and selectivity sequence of heavy metals by chicken bone-derived biochar: Batch and column experiment, *Journal of Environmental Science and Health, Part A*, 50 (2015), 1194-1204.

[41] A. P. Lim, A. Z. Aris, Continuous fixed-bed column study and adsorption modeling: Removal of cadmium (II) and lead (II) ions in aqueous solution by dead calcareous skeletons. *Biochemical engineering journal*, 87 (2014), 50-61.

[42] Z. Hseu, Z. Chen, C. Tsai, C. Tsui, S. Cheng, C. Liu, H. Lin, Digestion methods for total heavy metals in sediments and soils, *Water, Air, and Soil Pollution*, 141 (2002) 189-205.

[43] K.C. Uzoma, M. Inoue, H. Andry, H. Fujimaki, A. Zahoor, E. Nishihara, Effect of cow manure biochar on maize productivity under sandy soil condition, *Soil Use and Management*, 27 (2011) 205-212.

- [44] Y.S. Ho, G. McKay, Kinetic models for the sorption of dye from aqueous solution by wood, *Process Safety Environmental Protection*, 76 (1998) 183–191
- [45] Jr. W. J. Weber, J. C. Morris, J. Sanit, Kinetics of Adsorption on Carbon from Solution. *Journal of the Sanitary Engineering Division*, 89 (1963) 31-38.
- [46] S. Fan, Y. Wang, Z. Wang, J. Tang, J. Tang, X. Li, Removal of methylene blue from aqueous solution by sewage sludge-derived biochar: Adsorption kinetics, equilibrium, thermodynamics and mechanism, *Journal of Environmental Chemical Engineering*, 5 (2017) 601-611.
- [47] Q. Miao, E. Bi, B. Li, Roles of polar groups and aromatic structures of biochar in 1-methyl-3-octylimidazolium chloride ionic liquid adsorption: pH effect and thermodynamics study. *Environmental Science and Pollution Research*, 24 (2017) 22265-22274.
- [48] P. Saha, S. Chowdhury, *Insight Into Adsorption Thermodynamics*, INTECH Open Access Publisher, 2011.
- [49] B.H. Hameed, A.T.M. Din, A.L. Ahmad, Adsorption of methylene blue onto bamboo-based activated carbon: kinetics and equilibrium studies, *Journal of Hazardous Materials*, 141 (2007) 819–825.
- [50] M.B. Desta, Batch Sorption Experiments: Langmuir and freundlich isotherm studies for the adsorption of textile metal ions onto teff straw (*eragrostis tef*) agricultural waste, *Journal of Thermodynamics*, 2013 (2013) 1-6.

- [51] Itodo, A. U., Itodo, H. U., & Gafar, M. K. (2010). Estimation of specific surface area using Langmuir isotherm method. *Journal of Applied Sciences and Environmental Management*, 14(4).
- [52] Breviglieri, S. T., Cavaleiro, É. T. G., & Chierice, G. O. (2000). Correlation between ionic radius and thermal decomposition of Fe (II), Co (II), Ni (II), Cu (II) and Zn (II) diethanoldithiocarbamates. *Thermochimica acta*, 356(1-2), 79-84.
- [53] Ashcroft, N. W. (1966). Electron-ion pseudopotentials in metals. *Physics Letters*, 23(1), 48-50.
- [54] H.C. Thomas, Heterogeneous ion exchange in a flowing system, *Journal of the American Chemical Society*, 66 (1944) 1664–1666.
- [55] R. M. Clark, Evaluating the cost and performance of field-scale granular activated carbon systems, *Environmental science & technology*, 21 (1987) 573-580.
- [56] D. Özçimen, An approach to the characterization of biochar and bio-oil, *Renewable Energy for Sustainable Future*, iConcept Press, (2013) 41-58.
- [57] S. Sadaka, M. Sharara, A. Ashworth, P. Keyser, F. Allen, A. Wright, Characterization of biochar from switchgrass carbonization, *Energies*, 7 (2014) 548-567.
- [58] H. Böke, S. Akkurt, S. Özdemir, E.H. Göktürk, E.N.C. Saltik, Quantification of  $\text{CaCO}_3\text{-CaSO}_3\cdot 0.5\text{H}_2\text{O-CaSO}_4\cdot 2\text{H}_2\text{O}$  mixtures by FTIR analysis and its ANN model. *Materials Letters*, 58 (2004) 723-726.

- [59] A.W. Samsuri, F. Sadegh-Zadeh, B.J. Seh-Bardan, Characterization of biochars produced from oil palm and rice husks and their adsorption capacities for heavy metals, *International Journal of Environmental Science and Technology*, 11 (2014) 967-976.
- [60] M Thirumavalavan, Y.L. Lai, J.F. Lee, Fourier transform infrared spectroscopic analysis of fruit peels before and after the adsorption of heavy metal ions from aqueous solution, *Journal of Chemical Engineering Data*, 56 (2011) 2249–2255.
- [61] J.W. Lee, M. Kidder, B.R. Evans, S. Paik, A.C. Iii, C.T. Garten, R.C. Brown, Characterization of biochars produced from cornstovers for soil amendment, *Environmental Science & Technology*, 44 (2010) 7970-7974.
- [62] R. Subedi, N. Taupe, I. Ikoyi, C. Bertora, L. Zavattaro, A. Schmalenberger, C. Grignani, Chemically and biologically-mediated fertilizing value of manure-derived biochar, *Science of the Total Environment*, 550 (2016) 924-933.
- [63] J. Gomez-Eyles, L. Beesley, E. Moreno-Jimenez, U. Ghosh, T. Sizmur, The potential of biochar amendments to remediate contaminated soils, *Biochar and Soil Biota*, 4 (2013) 100-133.
- [64] R.R. Domingues, P.F. Trugilho, C.A. Silva, I.C.N.A. de Melo, L.C.A. Melo, Z.M. Magriotis, M.A. Sánchez-Monedero, Properties of biochar derived from wood and high-nutrient biomasses with the aim of agronomic and environmental benefits, *Plos One*, 12 (2017) 1-19.
- [65] J.W. Lee, A.C. Buchanan, B.R. Evans, M. Kidder, Oxygenation of biochar for enhanced cation exchange capacity, *Advanced Biofuels and Bioproducts*, Springer, New York, 2013.

- [66] N. Fiol, I. Villaescusa, Determination of sorbent point zero charge: usefulness in sorption studies, *Environmental Chemistry Letters*, 7 (2009) 79–84.
- [67] J.P. Simonin, On the comparison of pseudo-first order and pseudo-second order rate laws in the modeling of adsorption kinetics, *Chemical Engineering Journal*, 300 (2016) 254-263.
- [68] X. Chen, G. Chen, L. Chen, Y. Chen, J. Lehmann, M.B. McBride, A.G. Hay, Adsorption of copper and zinc by biochars produced from pyrolysis of hardwood and corn straw in aqueous solution, *Bioresource Technology*, 102 (2011) 8877-8884.
- [69] Z. Liu, F. Zhang, Removal of lead from water using biochars prepared from hydrothermal liquefaction of biomass, *Journal of Hazardous Materials*, 167 (2009) 933-939.
- [70] X. Chen, G. Chen, L. Chen, Y. Chen, J. Lehmann, M. B. McBride, A. G. Hay, Adsorption of copper and zinc by biochars produced from pyrolysis of hardwood and corn straw in aqueous solution, *Bioresource Technology*, 102 (2011), 8877-8884.
- [71] Y. Ding, Y. Liu, S. Liu, Z. Li, X. Tan, X. Huang, . . . X. Cai, Competitive removal of Cd(ii) and Pb(ii) by biochars produced from water hyacinths: performance and mechanism, *RSC Advances*, 6 (2016), 5223-5232.